AFFDL-TR-79-3042

AD A075215

LEVEL II

THE SCALING OF BIRD IMPACT LOADS

Antonios Challita
John P. Barber
University of Dayton Research Institute
300 College Park Avenue
Dayton, Ohio 45469

June 1979

TECHNICAL REPORT AFFDL-TR-79-3042
Final Report for Period 16 January 1978 - 16 February 1979

Approved for public release; distribution unlimited.

AIR FORCE FLIGHT DYNAMICS LABORATORY
AIR FORCE WRIGHT AERONAUTICAL LABORATORIES
AIR FORCE SYSTEMS COMMAND
WRIGHT-PATTERSON AIR FORCE BASE, OHIO 45433

79 10 19 043

NOTICE

When Government drawings, specifications, or other data are used for any purpose other than in connection with a definitely related Government procurement operation, the United States Government thereby incurs no responsibility nor any obligation whatsoever; and the fact that the Government may have formulated, furnished, or in any way supplied the said drawings, specifications, or other data, is not to be regarded by implication or otherwise as in any manner licensing the holder or any other person or corporation, or conveying any rights or permission to manufacture, use, or sell any patented invention that may in any way be related thereto.

This report has been reviewed by the Information Office (IO) and is releasable to the National Technical Information Service (NTIS). At NTIS, it will be available to the general public, including foreign nations.

This technical report has been reviewed and is approved for publication.

Robert E. McCarty
ROBERT E. MCCARTY
Project Engineer

R. Harley Walker
R. HARLEY WALKER
Group Leader
Subsystems Development Group

FOR THE COMMANDER

AMBROSE B. NUTT
Director
Vehicle Equipment Division

Copies of this report should not be returned unless return is required by security consideration, contractual obligations, or notice on a specific document.

AIR FORCE/56780/4 September 1979 — 150

UNCLASSIFIED

SECURITY CLASSIFICATION OF THIS PAGE (When Data Entered)

REPORT DOCUMENTATION PAGE

READ INSTRUCTIONS BEFORE COMPLETING FORM

1. REPORT NUMBER: AFFDL-TR-79-3042	2. GOVT ACCESSION NO.
3. RECIPIENT'S CATALOG NUMBER	
4. TITLE (and Subtitle): THE SCALING OF BIRD IMPACT LOADS	5. TYPE OF REPORT & PERIOD COVERED: Final Technical Report, 16 Jan [redacted]78 – 16 Feb [redacted]79
	6. PERFORMING ORG. REPORT NUMBER: UDR-TR-79-23
7. AUTHOR(s): Antonios Challita, John P. Barber	8. CONTRACT OR GRANT NUMBER(s): F33615-78-C-3402
9. PERFORMING ORGANIZATION NAME AND ADDRESS: University of Dayton Research Institute, 300 College Park Avenue, Dayton, Ohio 45469	10. PROGRAM ELEMENT, PROJECT, TASK AREA & WORK UNIT NUMBERS: Prog. Ele. 62201F, Proj. 2402, Task 240203, Work Unit 24020318
11. CONTROLLING OFFICE NAME AND ADDRESS: Air Force Flight Dynamics Laboratory, AF Wright Aeronautical Labs, AFSC, Wright-Patterson Air Force Base, OH 45433	12. REPORT DATE: Jun [redacted]79
	13. NUMBER OF PAGES: 67
14. MONITORING AGENCY NAME & ADDRESS (if different from Controlling Office)	15. SECURITY CLASS. (of this report): Unclassified
	15a. DECLASSIFICATION/DOWNGRADING SCHEDULE

18 6 10 9 14 15 11 12 67

16. DISTRIBUTION STATEMENT (of this Report)

Approved for public release; distribution unlimited.

17. DISTRIBUTION STATEMENT (of the abstract entered in Block 20, if different from Report)

16 2401 17 03

18. SUPPLEMENTARY NOTES

19. KEY WORDS (Continue on reverse side if necessary and identify by block number)

bird impact, birdstrike, impact loading, foreign object damage, modelling

20. ABSTRACT (Continue on reverse side if necessary and identify by block number)

This report describes an experimental study which was conducted to investigate the loads produced by the impact of 1800 g and 3600 g birds. Both real birds and bird simulants were tested. Impact pressures were measured and compared with smaller bird impact results obtained on previous testing programs. The magnitude of the impact pressures was found to be independent of bird size. The temporal and spatial distribution of impact pressures -

DD FORM 1 JAN 73 1473

UNCLASSIFIED

SECURITY CLASSIFICATION OF THIS PAGE (When Data Entered)

105 400

scaled linearly with bird dimensions. The impact behavior of large birds was consistent with flow models developed to describe small bird impacts. It was concluded that large and small birds display the same fundamental impact loading processes and that these processes are adequately described by the previously developed flow model.

FOREWORD

This report describes a contractual work effort conducted by personnel of the Impact Physics Branch, Experimental and Applied Mechanics Division, University of Dayton Research Institute, Dayton, Ohio under Project 2402, "Vehicle Equipment Technology," Task 240203, "Aerospace Vehicle Recovery and Escape Subsystems," Work Unit 24020318, "Simulation of Bird Impact on Aircraft Transparencies."

The work reported herein was performed during the period 16 January 1978 to 16 February 1979 under the direction of Dr. John P. Barber, the principal investigator. The Air Force project engineer was Mr. Robert E. McCarty (AFFDL/FER). The report was released by the authors in March 1979.

This report is one of three which will be published under contract number F33615-78-C-3402. The remaining two will deal with the effects of bird attitude upon impact loads, and development of a substitute bird for testing respectively and will be released as the work is completed.

TABLE OF CONTENTS

LIST OF ILLUSTRATIONS

PRECEDING PAGE BLANK

LIST OF ILLUSTRATIONS (CONT'D)

LIST OF SYMBOLS

a	Radius of projectile
ID	Inside diameter
m	Mass
OD	Outside diameter
P, P_p	Measured peak pressure
P_H	Hugoniot pressure
P_s	Stagnation pressure
r	Radial distance from center of impact
t	time
v, V	Impact velocity
V_n	Normal component of impact velocity
V_s	Shock velocity
ρ	Density of projectile
ρ_o	Density of material with zero porosity

LIST OF UNITS

Mass	g (gram)	$= 0.0022046\ lb_m$ (pound-mass)
	kg (kilogram)	$= 10^3 g$
Length	m (meter)	= 3.2808 ft (feet)
		= 39.37 in (inches)
	cm (centimeter)	= 0.01 m
		= 2.54 in
	mm (millimeter)	= 0.001 m
Time	s (second)	
	μs (microsecond)	$= 10^{-6} s$
Force	N (Newton)	$= 0.2248\ lb_f$ (pounds-force)
	MN (Meganewton)	$= 10^6 N$
Density	kg/m^3	$= 0.0624\ lb_m/ft^3$
		$= 3.613 \times 10^{-5}\ lb_m/in^3$
Pressure	MN/m^2	= 10 bars
		$= 145.04\ lb_f/in^2$
Frequency	H_z (hertz)	
	kH_z (kilohertz)	$= 10^3\ H_z$

SECTION I
INTRODUCTION

Collisions between birds and aircraft have proved to be an expensive and persistent problem to the United States Air Force. The severity of the problem has increased as high-speed, low-altitude aircraft missions have evolved. Windshield, canopy, and support structures have proved to be particularly vulnerable to birdstrike. Not only are these parts of the aircraft sensitive to impact damage, but the consequences of damage on pilot performance are severe. A number of aircraft and pilots have been lost due to birdstrike on windshields, canopies, and support structures.

The birdstrike vulnerability of the crew enclosure and transparencies in Air Force aircraft has resulted in a number of redesign programs. These redesign programs have usually been conducted in an iterative build and test mode. This method of design is extremely expensive and time consuming. The Air Force has, therefore, developed an interest in modern structural design techniques applied to the windshield birdstrike problem. This approach to the birdstrike design task involves the use of modern finite element structural analysis techniques. These techniques have been adapted to analyze the transient dynamic events such as birdstrike. The structural analysis techniques themselves have undergone extensive development over the years and have become highly reliable and efficient structural design tools. In order to adequately predict response, however, these techniques require good definition of the material properties and accurate descriptions of the transient impact loads. This report deals with the description of impact loads for use with finite element codes.

The University of Dayton Research Institute (UDRI) began work on the characterization of bird impact loads in January

of 1974. This work was jointly sponsored by the Air Force Materials Laboratory (AFML) and the Air Force Flight Dynamics Laboratory (AFFDL). A continuing effort has been conducted on the measurement and characterization of bird impact loads since that time. The original work, documented in Reference 1, developed the basic experimental techniques which were used throughout the program to obtain bird impact load data. This program concentrated on small birds (up to 120 g) and impacts at normal incidence. Work was continued on the measurement of small bird impact pressures. The data were more thoroughly analyzed and presented in Reference 2. This report identified the basic processes of bird impact and provided the first quantitative measurements of the pressures and forces involved. The work was extended and reported in Reference 3, which described in great detail the impact behavior of birds. Extensive data on birds weighing up to 600 g were reported. Some data for birds up to 4 kg were also obtained. The basic fluid behavior of birds during impact was identified and quantified. The development of the first satisfactory bird impact flow models was reported and the techniques necessary for proper scaling of the impact loads with bird size were identified. A more detailed theoretical base for bird impact modelling was described in Reference 4. This work presented a more detailed analysis of

---

[1] Barber, J.P. and J.S. Wilbeck, "The Characterization of Bird Impacts on a Rigid Plate: Part I," AFFDL-TR-75-5, ADA021142, January 1975.

[2] Peterson, R.L. and J.P. Barber, "Bird Impact Forces in Aircraft Windshield Design," AFFDL-TR-75-150, ADA026-628, March 1976.

[3] Barber, J.P., H.R. Taylor, and J.S. Wilbeck, "Bird Impact Forces and Pressures on Rigid and Compliant Targets," AFFDL-TR-77-60, ADA061-313, May 1978.

[4] Wilbeck, J.S., "Impact Behavior of Low Strength Projectiles," AFML-TR-77-134, ADA060-423, July 1978.

the basic process of bird impact and provides the theoretical basis for bird impact modelling as a fluid process. Additional impact work was conducted under an Air Force Aero Propulsion Laboratory contract and is reported in Reference 5. This report presented a much more careful experimental investigation of impact loads using simulated birds and ice. Careful measurements were made and agreement with prediction of the theoretical model was found to be excellent.

All of the work described above was conducted with, and based on, data produced with birds weighing 600 g or less. Although scaling derived from theoretical considerations worked extremely well over the range of bird masses from 60 g to 600 g, there was still some concern about the applicability of these models to birds with masses in the range from 1800 g to 3600 g. In particular, the 1800 g birds represent the standard design case for aircraft transparencies. It was, therefore, deemed necessary to collect experimental data on 1800 g and 3600 g birds to ensure that the theoretical models developed for use with structural element codes were applicable for this size bird. This report describes the experimental measurements made on 1800 g and 3600 g birds. The scaling relationships derived in the previous programs were checked and found to adequately describe the impact of these large birds.

---

[5] Bauer, D.P. and J.P. Barber, "Experimental Investigation of Impact Pressures Caused by Gelatin Simulated Birds and Ice," UDR-TR-78-114, November 1978.

SECTION II
EXPERIMENTAL TECHNIQUES

The experimental work described in this report was conducted at the University of Dayton Research Institute. This section contains a description of the experimental techniques used to obtain temporally resolved pressure measurements during bird impact onto a rigid plate. Descriptions of the experimental range and launch technique, target instrumentation, and data collection are given in the sections that follow.

2.1 LAUNCH TECHNIQUES

For experimental investigations of bird impact, a launch technique is necessary which can accelerate birds of the required mass to the required velocities. The birds must be launched with controlled orientation (preferably with zero pitch and yaw), and such that they do not break up or severely distort prior to impact. A launch technique was developed with which birds of up to 3.6 kg could be launched to velocities up to approximately 300 m/s.

The system consisted of a 177.8 mm bore compressed air gun with supporting compressor, instrumentation, and control systems. The compressor system consisted of a 1.42 m^3/min, 3.5 MN/m^2 compressor pumping into a 0.11 m^3 intermediate storage tank. The intermediate storage tank was connected via a flexible hose and quick disconnect coupler to the large air storage tank used for driving the gun. The driving air storage tank had a capacity of approximately 0.85 m^3. There was a valve system located between the driving air storage tank and the breech of the gun. This valve system was designed to valve the high pressure air from the driving storage tank into the gun to

operate the gun. The valve was a standard butterfly valve system with a pneumatic actuator. The breech end of the gun, together with the compressor storage tank and driving tank systems, is shown in Figure 1.

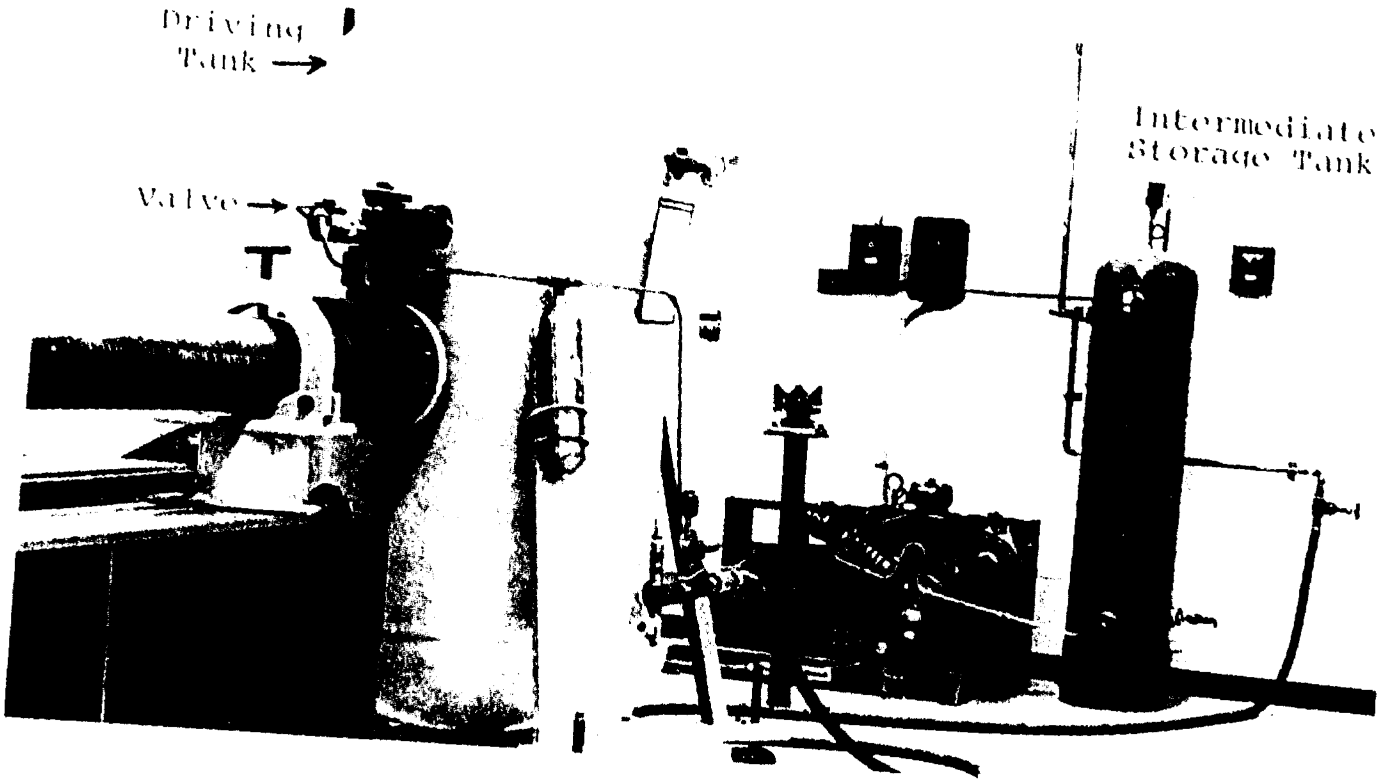

Figure 1. Compressor Storage Tank and Driving Tank Systems

The gun itself consisted of two, 4.88 m long, 177.8 mm ID heavy wall tubes. They were connected together via a locating ring and flange system. The tubes were supported on two heavy I-beams bolted to the floor. A vent section was connected to the muzzle of the gun tube and was designed to release the driving pressure from the back of the projectile package. This vent section was enclosed in a muffler which deflected the venting gases harmlessly towards the floor.

The birds were placed in a sabot, or carrier, for launching. The sabot was a 177.8 mm OD foam plastic cylinder. Foam plastic was employed, as a substitute of balsa wood, after identifying

several unsatisfactory characteristics of the original balsa wood sabots. There is only one supplier of balsa wood in the United States, and the sizes and quantities which could be supplied were only marginally satisfactory for these large sabots. 180 mm balsa planking was not available, so up to nine smaller planks had to be bonded together to form a work piece large enough to fabricate these sabots. This fabrication technique produced sabots which were only marginally strong enough. They often broke during fabrication. The molded plastic sabots proved completely satisfactory for launching birds over the range of sizes and velocities used in this study. They are light, strong and very dimensionally stable.

As the sabot represents a significant fraction of the launch mass, it must be stripped from the bird before the bird impacts the target. Accordingly, a tapered tube sabot stripping section was connected to the muzzle end of the vent section. The sabot stripper tube consisted of a steel tube with an initial ID of 177.8 mm that was progressively reduced. A series of longitudinal wide slots were cut into the stripper tube to facilitate the rapid release of the driving pressure, thus reducing the forces required to decelerate and stop the sabot. When the launch package entered the sabot stripper tube, the sabot was progressively decelerated until it stopped. The bird released from the sabot pocket and continued on trajectory to the target. For the high velocity shots, an extension to the stripper tube was required. It consisted of nine bars welded around a ring and connected to the stripper tube through a flange system. The vent section muffler and stripper tube are shown in Figure 2. The sabot stripper functioned satisfactorily over the entire range of masses and velocities which were used in this program.

Free flight observations of the bird showed that the bird was oscillating after sabot separation. This oscillation was apparently initiated by the release of the bird from the sabot. To assist in the smooth release of the bird, holes were drilled in the base of the sabot. These holes permit the driving pressure

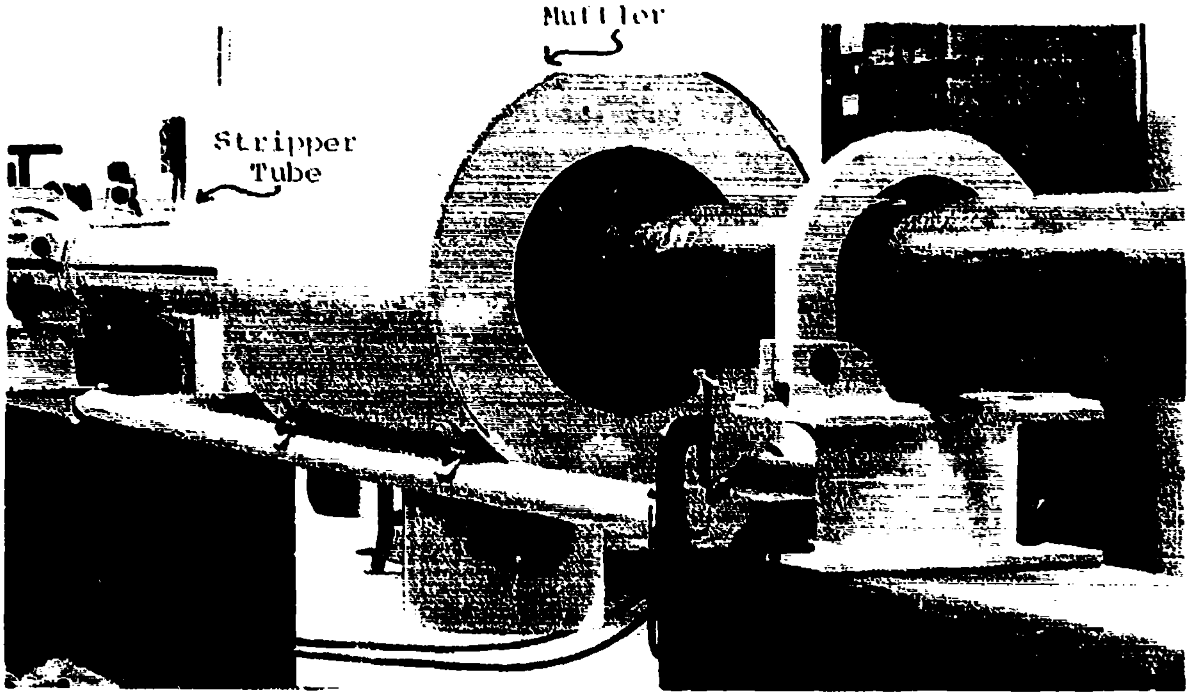

Figure 2. The Vent Section Muffler and Stripper Tube

to act on the base of the bird itself. Therefore, the bird was both pushed and pulled out of the sabot during the separation process. This technique appeared to greatly reduce the bird oscillation problem.

2.2 VELOCITY, LOCATION, AND ORIENTATION MEASUREMENT

The velocity of the bird was measured prior to impact using a simple time of flight technique. Between the muzzle of the sabot stripper and the target, two helium/neon laser beams were directed across the trajectory. When the bird interrupted the first laser beam, a counter was started. The counter was stopped when the bird interrupted the second laser beam. The distance between the laser beams and the elapsed time were used to calculate the velocity. To increase the accuracy of the velocity measurements, monitor bird orientation, determine projectile impact location on target, and verify bird integrity

prior to impact, two orthogonal pulsed x-ray systems were set up at each laser beam station. The resulting radiographs of the bird in flight were used to accurately establish the position of the bird with respect to the laser beam and to monitor the condition and orientation of the bird. The accurate determination of projectile location and orientation relative to the target is necessary to properly describe the pressure distribution. Using this technique, velocities could be measured to within one percent, projectile impact location on target could be determined to within about 1.25 cm, and orientation to within ±0.5 degrees. Bird disintegration during launch was extremely rare and was not an experimental problem. The instrumentation described above is shown in Figure 3.

2.3 PRESSURE MEASUREMENTS AND RECORDING

The impact shock pressures can be extremely high, the duration of the impact is relatively short and there could be important transient pressure excursions. The pressure sensing devices must be capable of measuring and withstanding these high pressures and the pressure sensing and recording equipment must have adequate bandwidth to detect and record important pressure transients.

Piezoelectric quartz pressure transducers were used as the basic sensing devices for these experiments. These transducers have a compact impedence converter physically located in the coaxial line close to the crystal, and they have a specified bandwidth from 0 to 80 kHz. Since these transducers are not specifically designed for impact testing, calibration was necessary to verify their operation. In Reference 1 Barber gives details of calibration techniques in his report. The

[1]Barber, J.P. and J.S. Wilbeck, "The Characterization of Bird Impacts on a Rigid Plate: Part I," AFFDL-TR-75-5, ADA021142, January 1975.

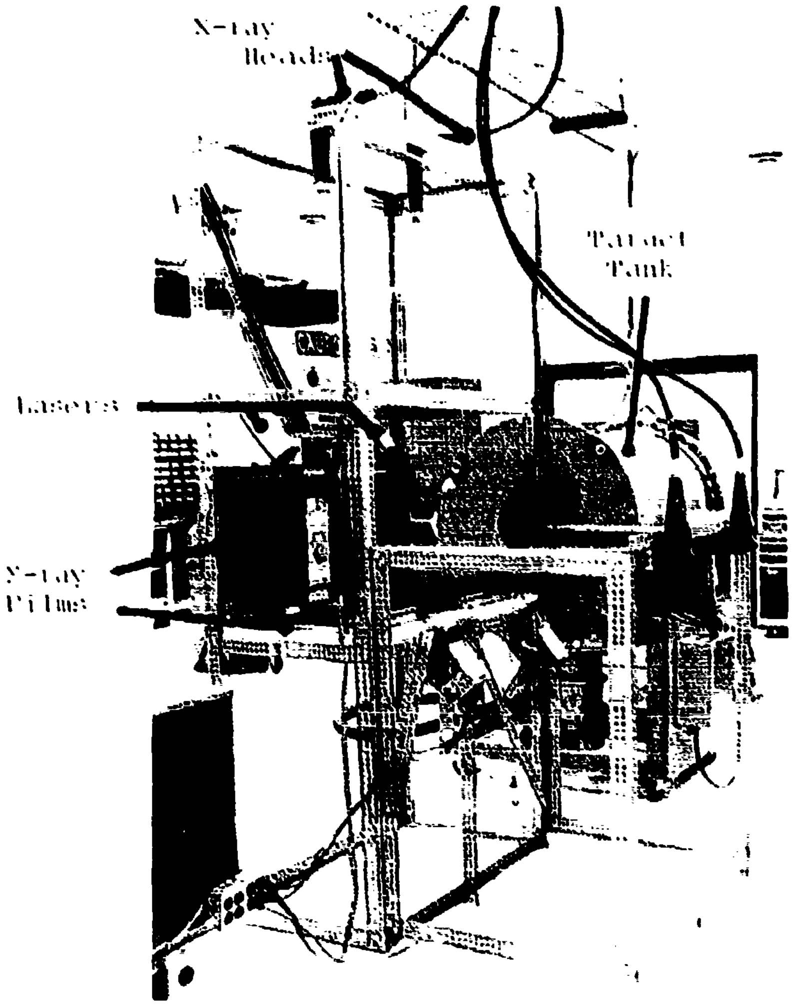

Figure 3. Instrumentation Section

transducers were mounted flush with the surface of a heavy steel plate. Up to nine transducers were simultaneously mounted in the plate on orthogonal axes.

The pressure signals were recorded using an electronic digital memory system. This system uses an analog to digital signal converter. The system has a 200 kHz sample rate, and each channel can store 2048 data points in shift registers. The pressure signals were displayed on an oscilloscope, as a function

of time, and the time interval of interest determined. Then, digital data over these intervals was recorded on a cassette and could be printed out on an electronic data terminal. This technique significantly increased the accuracy and reliability of the data.

SECTION III

EXPERIMENTAL RESULTS

A total of 83 data shots were performed to investigate the scaling of bird impact loads. The objective was to demonstrate that the scaling relationships which worked extremely well over the range of bird masses from 60 to 600 g, were applicable to bird masses ranging from 1800 to 3600 g. The projectiles used in these tests included birds (chickens) and bird substitutes (porous gelatin). They were impacted at three impact angles (90°, 45°, 25°) and at velocities ranging from 100 m/s to 300 m/s. The substitute birds were right circular cylinders with a length to diameter ratio of approximately two.

The time varying pressure data were collected using a digital data memory system as described in Section II. From these recorded data, measurements were made to obtain peak pressure and steady flow pressure. The results of these measurements together with comparisons to theoretical results and measurements from impacts of smaller size birds and bird substitutes reported by Barber in Reference 3 and Bauer in Reference 5 are presented in the following sections.

3.1 INTRODUCTION

Birds independent of their masses can be assumed to be right circular cylinders with a length to diameter ratio greater

---

[3]Barber, J.P., H.R. Taylor, and J.S. Wilbeck, "Bird Impact Forces and Pressures on Rigid and Compliant Targets," AFFDL-TR-77-60, ADA061-313, May 1978.

[5]Bauer, D.P. and J.P. Barber, "Experimental Investigation of Impact Pressures Caused by Gelatin Simulated Birds and Ice," UDR-TR-78-114, November 1978.

than two, and to behave like fluids during impacts. These two basic assumptions provide the basis for understanding the scaling of bird impact loads.

Because the impact process is basically fluid dynamic, the characteristic pressures are the Hugoniot, or impact, pressure and the flow, or stagnation, pressure. Both of these pressures depend only on the impact velocity and the material properties of the bird (i.e., density and shock velocity). The magnitudes of these pressures should not vary with bird size, however, the spacial and temporal distribution of pressure should. Since birds of different mass are, however, geometrically similar (i.e., they have similar length to diameter ratios), pressure distributions should scale linearly with bird dimensions. That is, pressure distributions should depend only on normalized distances (where normalization is carried out with a bird dimension such as diameter or length). This was, in fact, shown in Reference 3 for birds and Reference 5 for substitute birds up to 600 g.

Bird and gelatin impacts on a steel target plate may be considered as soft body impacts since the stresses generated during impact substantially exceed the strength of the projectile but are well below the strength of the target material. Pressure records obtained from such impacts are shown in Figure 4, 5 and 6. Figures 4 and 5 show typical pressure traces from normal and oblique impact of a nominal 1800 g and 3600 g right circular cylindtical gelatin projectile. Figure 6 shows similar pressure traces from impacts of a real bird (chicken). The two pressure

---

[3] Barber, J.P., H.R. Taylor, and J.S. Wilbeck, "Bird Impact Forces and Pressures on Rigid and Compliant Targets," AFFDL-TR-77-60, ADA061-313, May 1978.

[5] Bauer, D.P. and J.P. Barber, "Experimental Investigation of Impact Pressures Caused by Gelatin Simulated Birds and Ice," UDR-TR-78-114, November 1978.

V = 105 m/s
m = 1750 g
P = 18.5 MN/m^2-cm
t = 2000 μs/cm

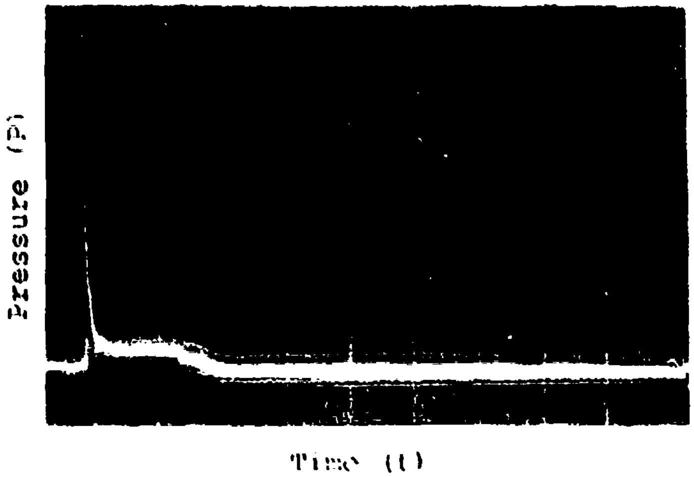

(a)

V = 199 m/s
m = 1840 g
P = 14.5 MN/m^2-cm
t = 2000 μs/cm

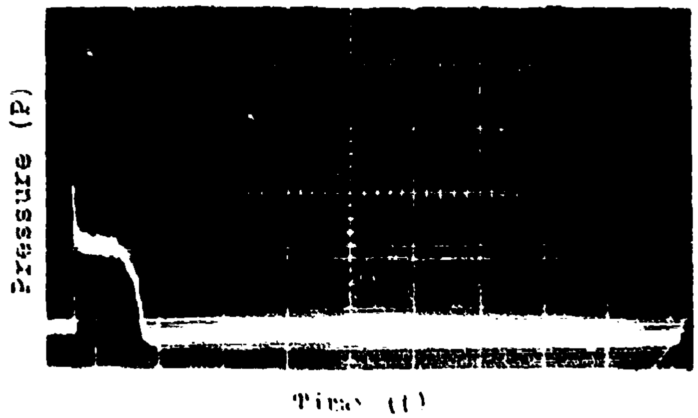

(b)

V = 203 m/s
m = 1800 g
P = 13.1 MN/m^2-cm
t = 2000 μs/cm

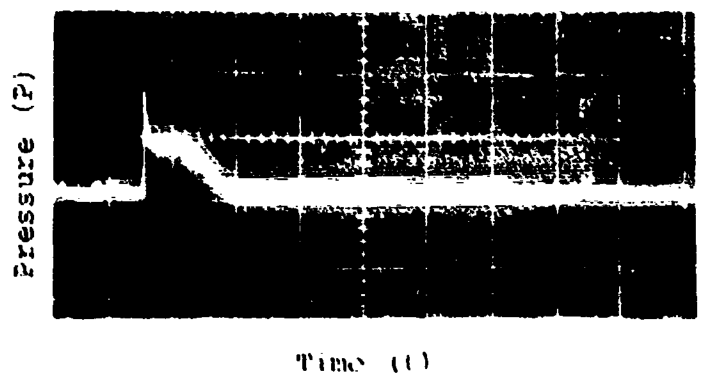

(c)

Figure 4. Typical Pressure-Time Record of Nominal 1800 g Gelatin with 10% Porosity. (a) 90° impact, center transducer; (b) 45° impact, 3" below center; (c) 25° impact, center transducer.

V = 245 m/s
m = 3220 g
P = 32.8 MN/m^2-cm
t = 2000 μs/cm

Pressure (P)

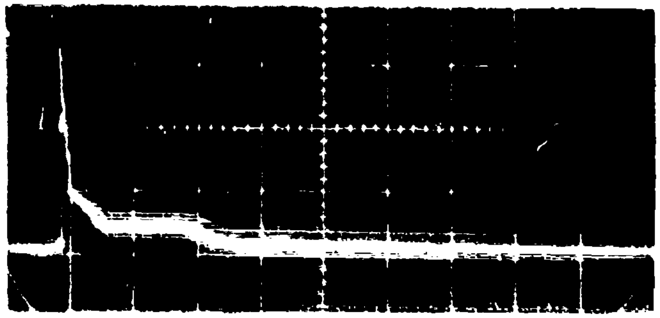

(a)

Time (t)

V = 115 m/s
m = 3490 g
P = 16.6 MN/m^2-cm
t = 2000 μs/cm

Pressure (P)

(b)

Time (t)

V = 190 m/s
m = 3550 g
P = 13.1 MN/m^2-cm
t = 2000 μs/cm

Pressure (P)

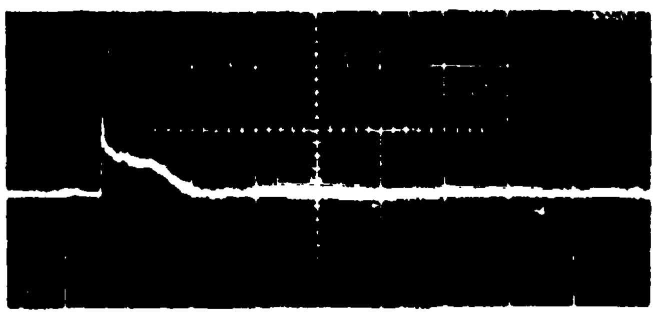

(c)

Time (t)

Figure 5. Typical Pressure-Time Record of Nominal 3600 g Gelatin with 10% Porosity. (a) 90° impact, 1" above center; (b) 45° impact, center transducer; (c) 25° impact, center transducer.

V = 289 m/s
m = 1560 g
P = 46.3 MN/m^2-cm
t = 2000 μs/cm

V = 104 m/s
m = 1560 g
P = 5.2 MN/m^2-cm
t = 2000 μs/cm

V = 273 m/s
m = 1560 g
P = 13.1 MN/m^2-cm
t = 2000 μs/cm

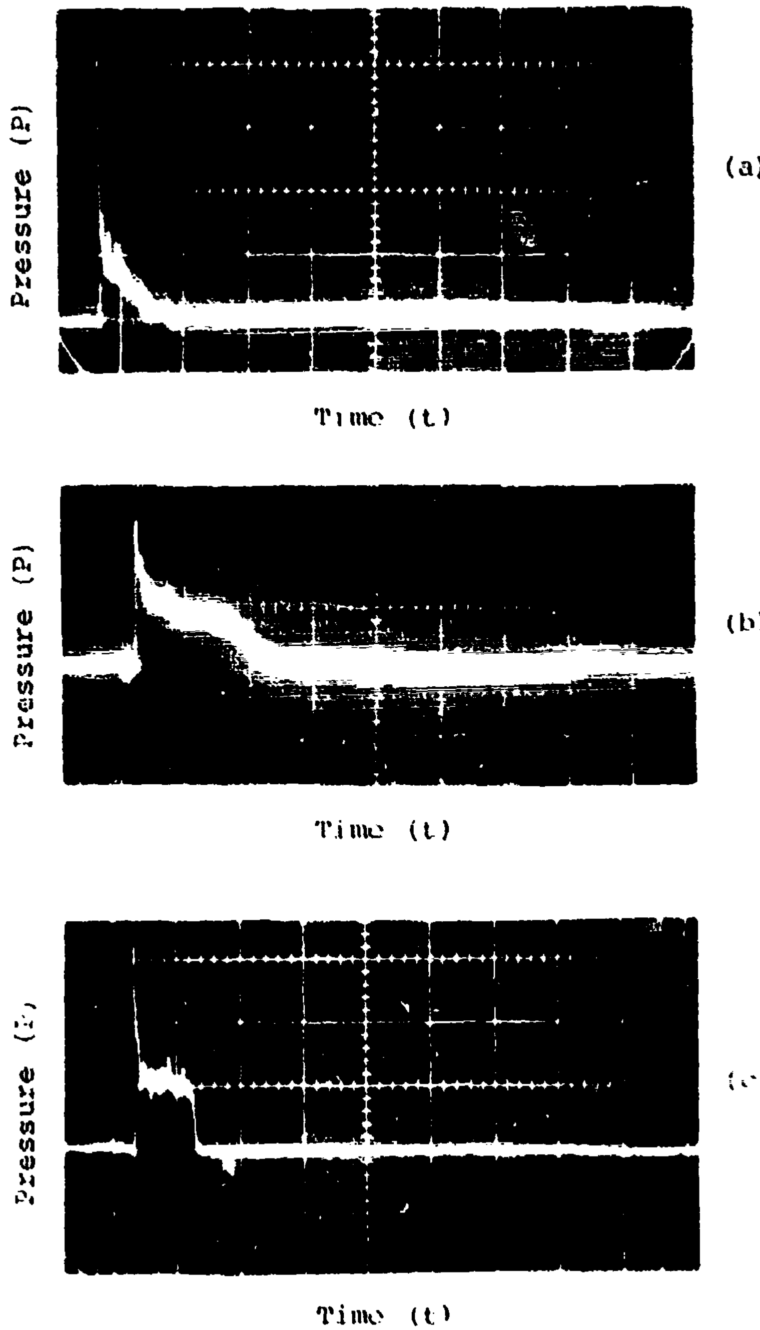

Figure 6. Typical Pressure-Time Record of Nominal 1800 g Real Bird (chicken). (a) 90° impact, center transducer; (b) 45° impact, center transducer; (c) 25° impact, center transducer.

levels of interest on these traces are the peak pressure and the steady flow pressure.

The peak pressure is due to a shock wave formed from the initial impact, and is mainly a function of the normal component of impact velocity and the projectile's properties. The steady flow pressure occurs when the initial shock wave is overtaken by the release waves formed from the pressure gradient along the projectile's edge. The phases of the impact process are shown in Figure 7.

3.2 IMPACT DURATION

The time duration of impact of birds was first derived by Barber in Reference 3 and was found to equal the projectile length divided by the impact velocity. The same results were found during this experimental program. These results also agree with the results presented by Bauer in Reference 5 during his experimental investigation on simulated birds.

3.3 INITIAL IMPACT PRESSURE

During the initial impact, the particles on the front surface of the projectile are instantaneously brought to rest relative to the target face and a shock propagates into the projectile. As the shock wave propagates into the projectile, it brings the material behind the shock to rest. The pressure in the shock compressed region is initially very high and is uniform across the impact area. The pressure behind the shock,

---

[3]Barber, J.P. and H.R. Taylor, and J.S. Wilbeck, "Bird Impact Forces and Pressures on Rigid and Compliant Targets," AFFDL-TR-77-60, ADA061-313, May 1978.

[5]Bauer, D.P. and J.P. Barber, "Experimental Investigation of Impact Pressures Caused by Gelatin Simulated Birds and Ice," UDR-TR-78-114, November 1978.

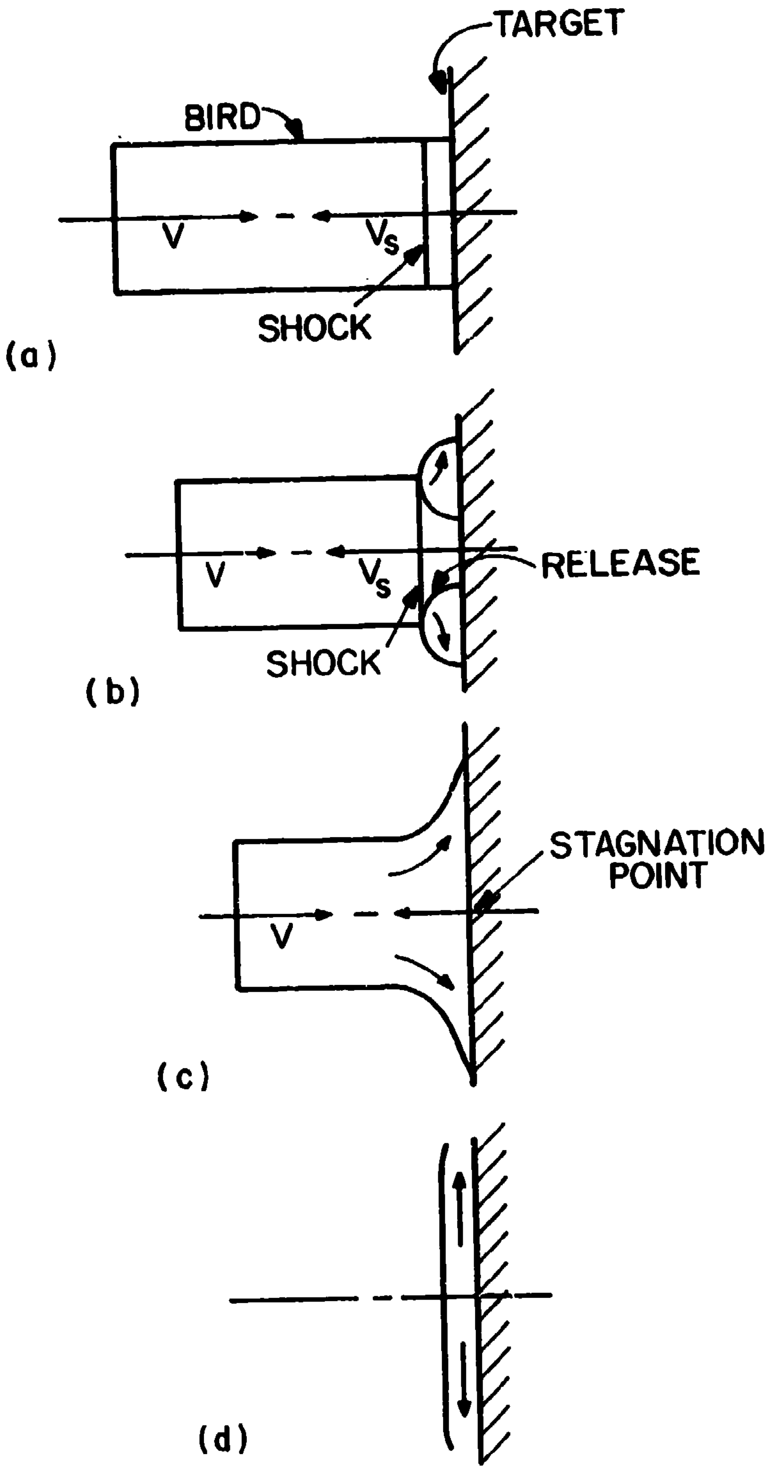

Figure 7. The Phases of Bird Impact: (a) Initial Impact, (b) Impact Decay; (c) Steady Flow; and (d) Termination

(the Hugoniot pressure) is:

$$P_H = \rho V_s V_n \qquad (1)$$

where ρ is the density of the projectile, V_s is the shock velocity, and V_n is the normal component of impact velocity. The relation between the shock velocity V_s and the normal component of impact velocity V_n for gelatin with 10 percent porosity was derived by Wilbeck in Reference 4. The initial impact pressures measured for all normal and oblique impacts for bird and gelatin are presented in Figures 8, 9, and 10. The measured impact pressures for normal impact for nominal 1800 g real bird agree very well with the calculated pressures. The agreement is better than the experimental results from small birds reported by Barber in Reference 3. The small bird data were probably affected by the limited bandwidth (80 kHz) of the transducers. The shock pulse was barely defined for the large birds (see Figures 4-6). Shock pulse duration was only about half as long for the small bird impacts, and the peaks may have been clipped. The measured shock pressures for normal impact for gelatin with 10 percent porosity are well above those anticipated. The shock pressures approached those expected for pure gelatin and were up to twice as high as those expected for the porous gelatin bird simulant material. A thorough investigation was conducted and the source of these extremely high and unexpected pressures was determined and eliminated during the later shots.

It was found that the part of the bird initially striking the target was essentially pure gelatin. Birds were launched

---

[4] Wilbeck, J.S., "Impact Behavior of Low Strength Projectiles," AFML-TR-77-134, ADA060-423, July 1978.

[3] Barber, J.P., H.R. Taylor, and J.S. Wilbeck, "Bird Impact Forces and Pressures on Rigid and Compliant Targets," AFFDL-TR-77-60, ADA061-313, May 1978.

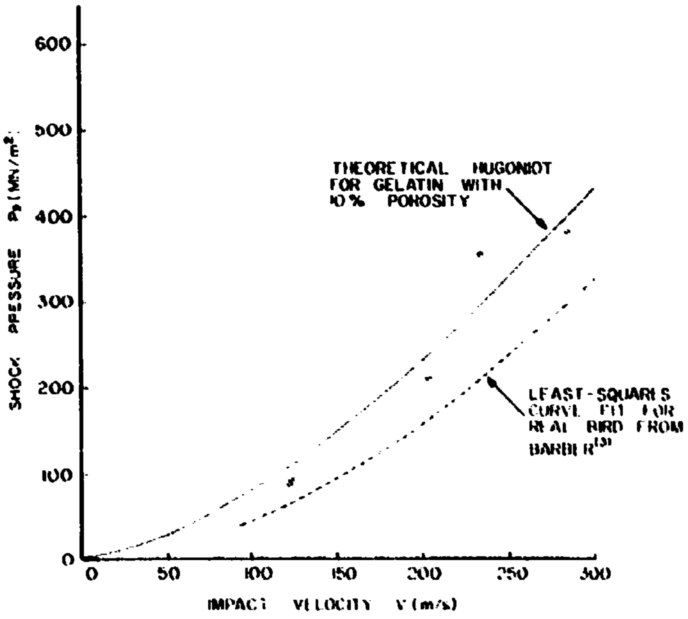

Figure 8a. Initial Impact (Hugoniot) Pressures versus Impact Velocity for Nominal 1800 g Real Bird (chicken) at Normal Impact

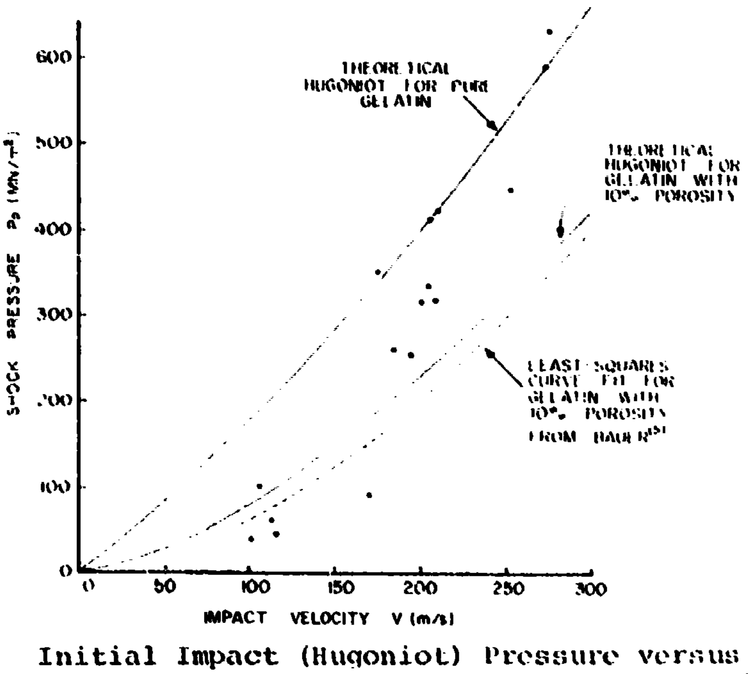

Figure 8b. Initial Impact (Hugoniot) Pressure versus Impact Velocity for Nominal 1800 g and 3600 g Gelatin at Normal Impact. Points show data from this program.

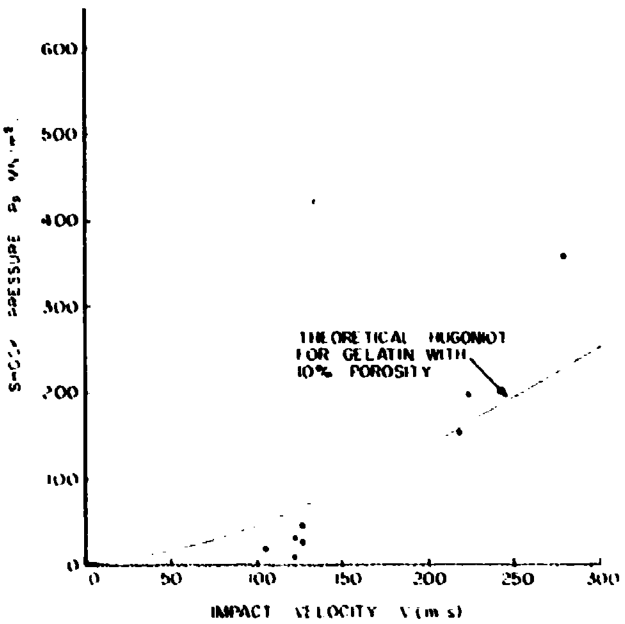

Figure 9a. Initial Impact (Hugoniot) Pressures Versus Impact Velocity for Nominal 1800 g Real Bird (chicken) at 45° Impact

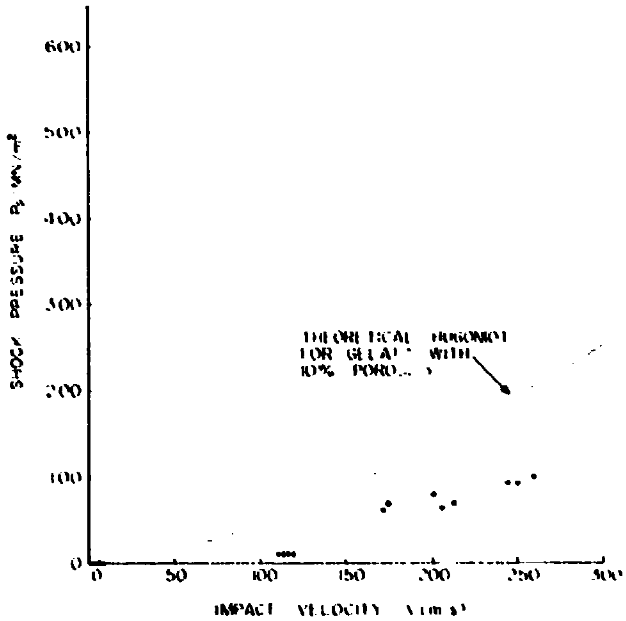

Figure 9b. Initial Impact (Hugoniot) Pressures Versus Impact Velocity for Nominal 1800 g and 3600 g Gelatin with 10 Percent Porosity at 45° Impact

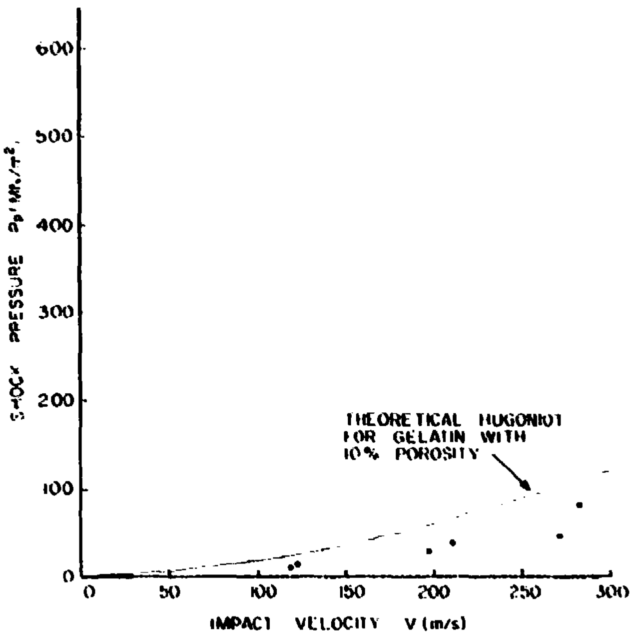

Figure 10a. Initial Impact (Hugoniot) Pressures versus Impact Velocity for Nominal 1800 g Real Bird (chicken) at 25° Impact

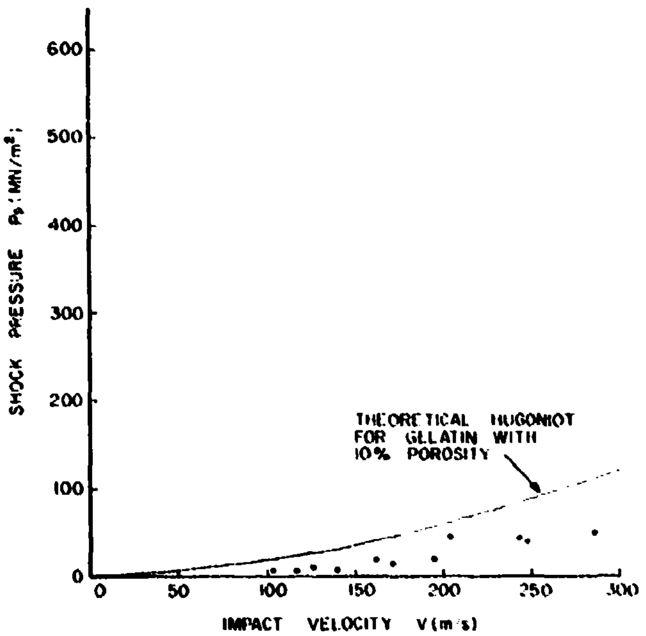

Figure 10b. Initial Impact (Hugoniot) Pressures versus Impact Velocity for Nominal 1800 g and 3600 g Gelatin at 25° Impact.

such that the end of the bird which first struck the target was the end that was at the bottom of the mold during the molding process. The presence of pure gelatin at the bottom of the mold was due to the tendency of the phenolic microballoons, which were used to provide porosity, to float out of the gelatin during the curing process. This was confirmed by making density measurements along the axis of the bird. The results for several processes are shown in Figure 11. Pure gelatin was found at the bottom of the mold and extremely low density gelatin at the top of the mold. Numerous different processing techniques were tried in an attempt to eliminate the density gradients from the bird. As can be seen from Figure 11, good density uniformity was obtained in many cases but in general the density was too low. Efforts to increase density always resulted in increased density gradients. As a result of this investigation, birds were molded some 30 percent longer than the nominal bird length and approximately 15 percent was trimmed from each end. This technique produced density variations which fell between acceptable limits. To further insure that the very high peak pressures were not produced, birds were launched top end (low density end) first. These changes produced better behavior in the later oblique shots. The measured impact pressures for oblique impact for gelatin and real birds are, as expected, lower than the calculated values. In addition, low recorded peak pressure during oblique impacts may have also been caused by the relatively shorter duration of the shock pulse in these impacts. As pointed out earlier, the limited bandwidth of the transducers can result in a significant attenuation of the measured signals. For 25° and 45° impacts, the initial impact pressure spike was much less pronounced than for 90° impacts.

3.4 STEADY FLOW PRESSURES

As the shock wave propagates into the projectile, the material at the edge of the projectile is subjected to a very high pressure gradient. This pressure gradient causes the

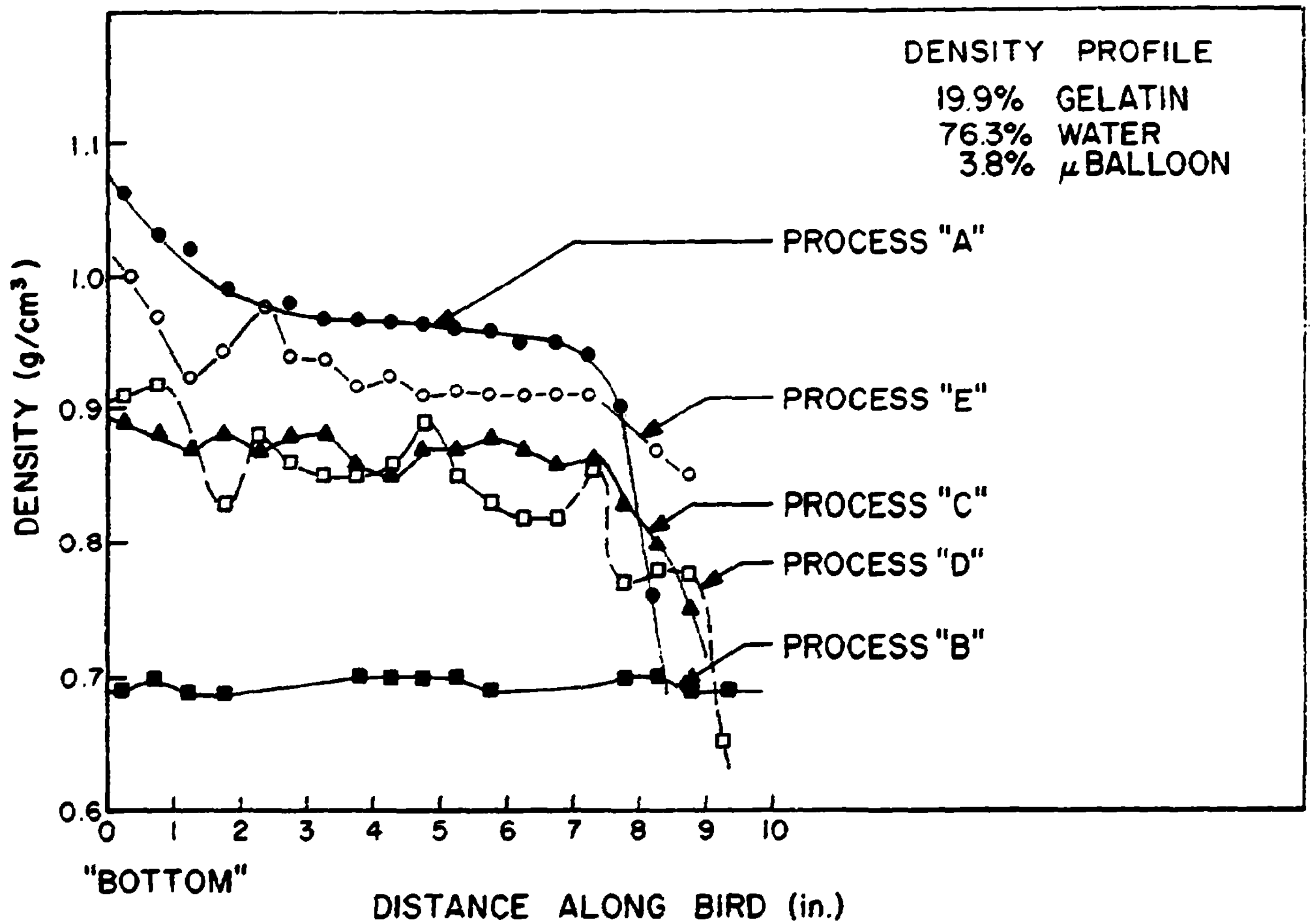

Figure 11. Density Profiles for 4lb Simulant Birds Prepared with Different Techniques

material to be accelerated radially outward, and release waves propagate inward. The function of these release waves is to relieve the radial pressure gradient in the projectile. Release waves travel into the projectile, eventually overtaking the initial shock wave. The release process for a cylinder is shown in Figure 12. As the radial pressure decreases during the shock pressure decay, shear stresses develop in the projectile material. These shear stresses are greater than the shear strength of the material and are sufficient to cause "flow". Then, the bird can be considered to behave as a fluid. After several reflections of the release waves, a condition of steady flow is established. A constant pressure and velocity field is set up in the projectile and remains until the end of the projectile reaches the target surface. This steady-state phase is usually indicated by a pressure plateau on the pressure traces. As could be seen in Figures 4, 5, and 6, a large amount of high frequency "noise" was superimposed on the pressure profiles, which made it hard to identify the plateau and to make an accurate measurement of steady-state pressure. Therefore, an average value of the pressure was measured and used in presenting the pressure distributions. This noise was investigated in Reference 4 by Wilbeck and might have been caused by the break-up or tearing of the material (creation of new surfaces) during impact or by the acceleration loads on the gages caused by the pressure plate vibrations.

Using potential flow theory, Wilbeck calculated, in Reference 4, the steady-state pressure for a bird impact at normal incidence. The pressure at the center of impact was found to equal the stagnation pressure which was approximated by:

$$P_s = \frac{1}{2} \rho_o v^2 \qquad (2)$$

---

[4]Wilbeck, J.S., "Impact Behavior of Low Strength Projectiles," AFML-TR-77-134, ADA060-423, July 1978.

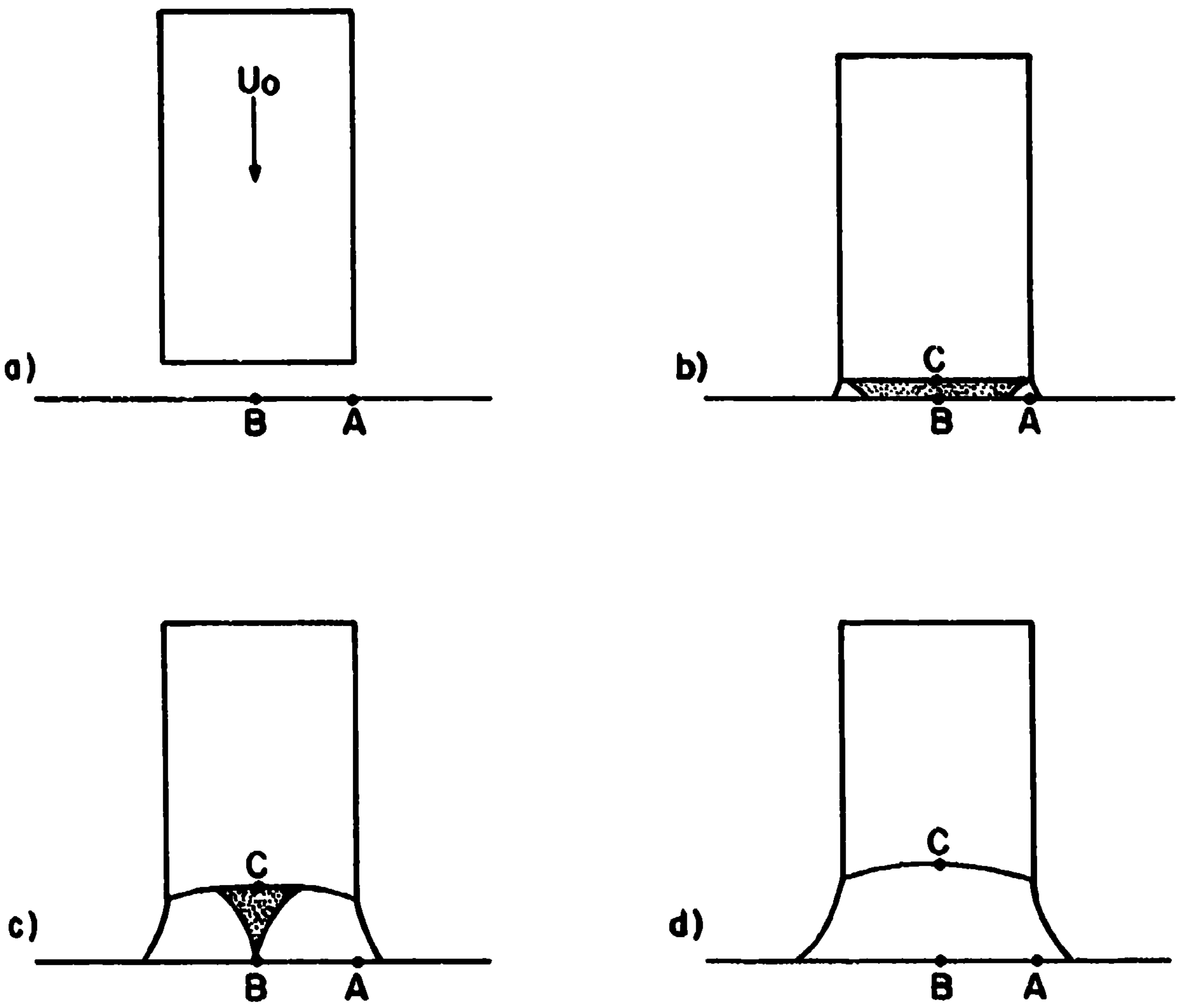

Figure 12. Shock and Release Waves in Fluid Impact. (a) before impact; (b) shocked region just after impact; (c) release waves have converged on Point B, the axis of the cylinder; (d) release waves have just caught the center of the shock, Pt. C.

where ρ_o is the density of the material with zero porosity and v is the impact velocity. The stagnation pressure is the highest pressure during the steady flow regime and is an important factor in scaling bird impact loads, since it is used to nondimensionalize the steady flow pressure distribution.

For oblique impact, the majority of fluid will flow "downstream" on the obtuse side of the impact. The stagnation point shifts "upstream" to the acute side of the center of impact as shown in Figure 13. As long as a stagnation point exists, the

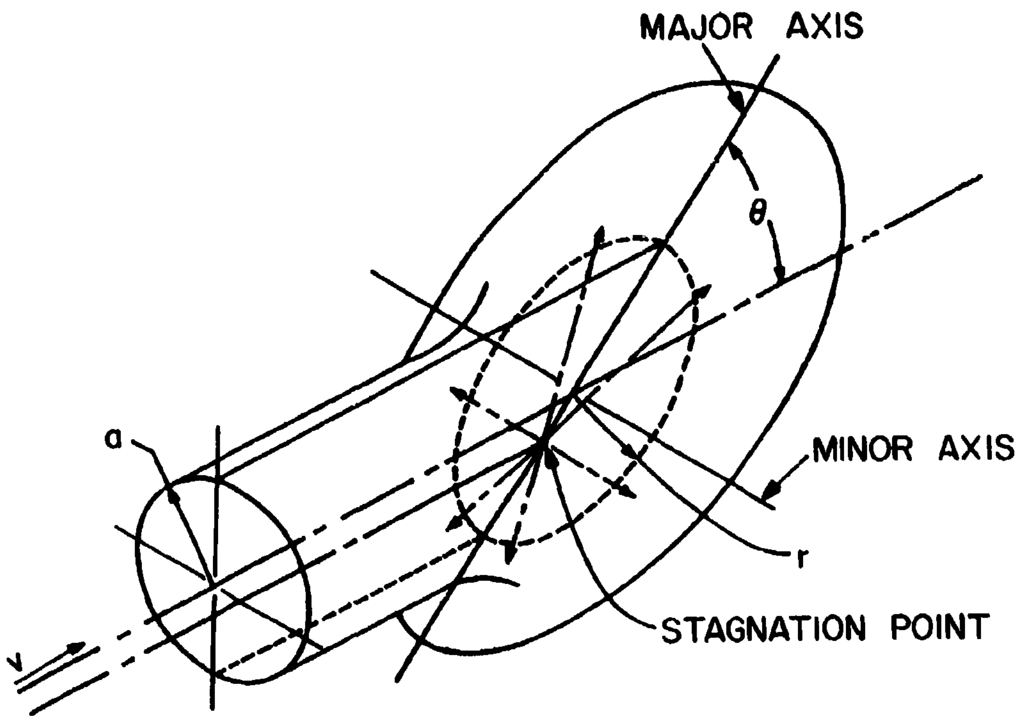

Figure 13. Flow Geometry at Oblique Impact

full stagnation pressure will occur at the stagnation point regardless of angle of impact. However, the distribution of pressure along the surface will be greatly dependent on the impact angle. The distribution of pressure in an oblique cylindrical impact is difficult to analyse because it is a

three-dimensional fluid dynamic problem. In Reference 6, Boehman used potential flow theory to develop a computer model for predicting the pressure distribution produced by the steady state flow of a cylindrical jet impacting on a rigid flat plate. The code utilizes a source density distribution on the surface of the plate and solves for the pressure distribution necessary to make the normal velocity zero on the boundary. Originally, the input to this program consisted of the coordinates of points describing the body surface. For our purposes, the code was modified to generate a grid describing the plate, where the size of the grid depends on the mass of the bird and the angle of impact. A listing of the modified code along with a sample input and output data is presented in the Appendix. The experimental pressure data measured in this task is compared to those theoretical curves and to the experimental data from Reference 3 by Barber and Reference 5 by Bauer in the following sections.

3.4.1 Gelatin Artificial Birds

Figures 14, 15, and 16 show the nondimensionalized steady flow pressure distributions along the major axis produced by gelatin with 10 percent porosity for 90°, 45°, and 25° impact angles, respectively. The pressures are normalized to the stagnation pressure as calculated in Equation (2). Together with the experimental data, two sets of curves are shown in these figures. The predicted pressure distribution from

---

[6] Boehman, L.I., and A. Challita, "A Model for Predicting Bird and Ice Impact Loads on Structures," UDR-TR-79-54.

[3] Barber, J.P., H.R. Taylor, and J.S. Wilbeck, "Bird Impact Forces and Pressures on Rigid and Compliant Targets," AFFDL-TR-77-60, ADA061-313, May 1978.

[5] Bauer, D.P. and J.P. Barber, "Experimental Investigation of Impact Pressures Caused by Gelatin Simulated Birds and Ice," UDR-TR-78-114, November 1978.

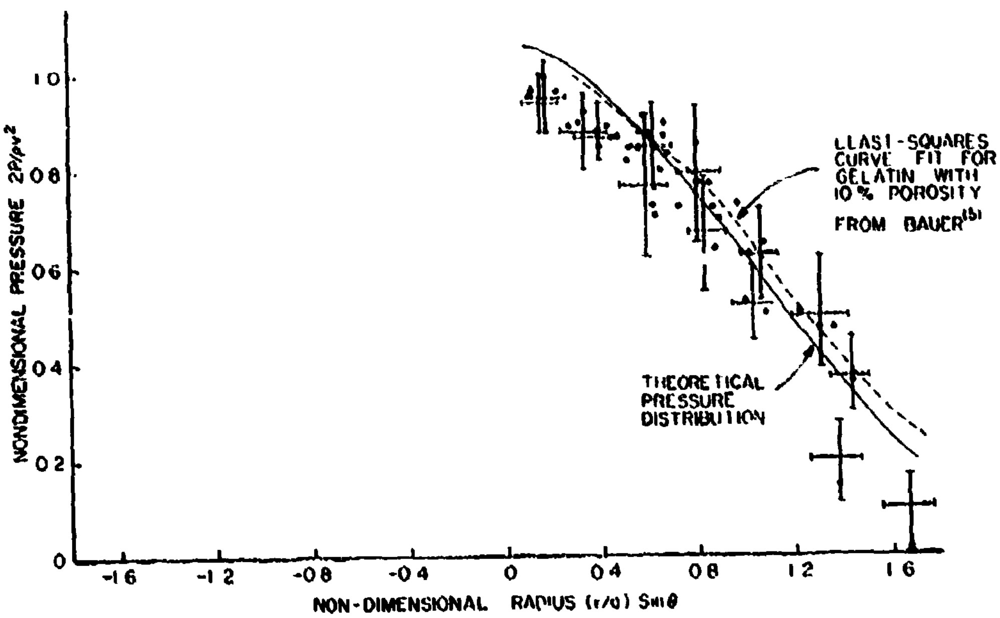

Figure 14. Normalized Steady Flow Pressure Distribution of Nominal 1800 g and 3600 g Gelatin with 10% Porosity Along Major Axis at Normal Impact

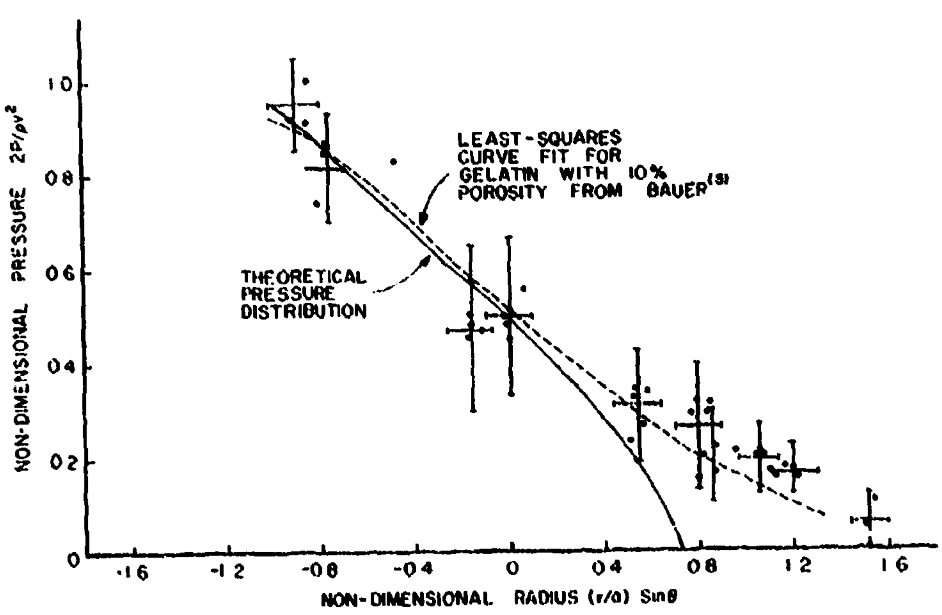

Figure 15. Normalized Steady Flow Pressure Distribution of Nominal 1800 g and 3600 g Gelatin with 10% Porosity Along Major Axis at 45° Impact

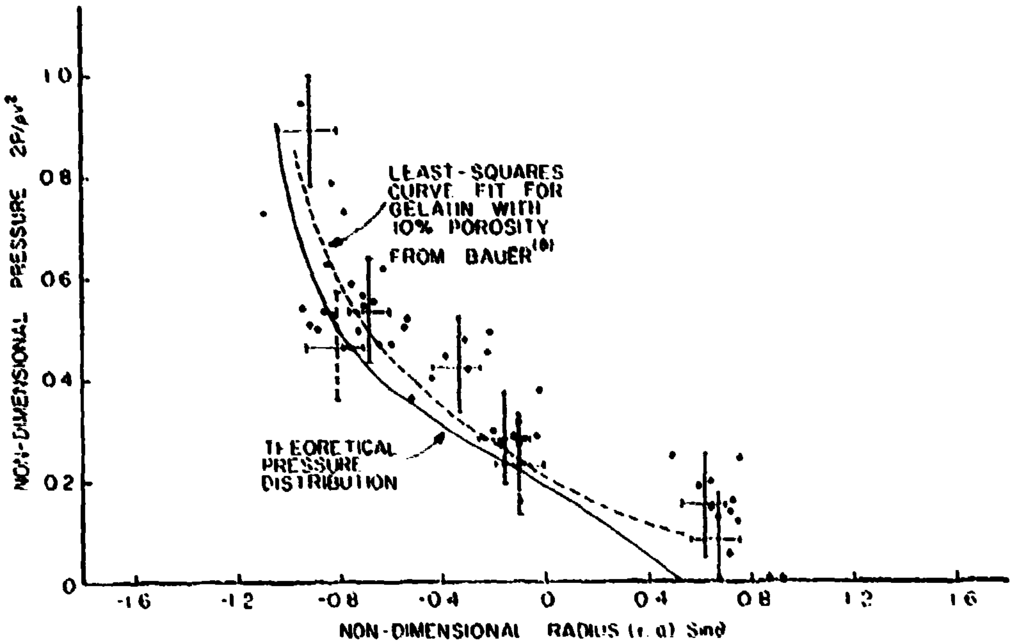

Figure 16. Normalized Steady Flow Pressure Distribution of Nominal 1800 g and 3600 g Gelatin with 10% Porosity Along Major Axis at 25° Impact

Reference 6 by Boehman for normal (90°), 45°, and 25° impacts, and the least-squares curve fits of the experimental data for smaller size gelatin projectiles from Reference 5 by Bauer. The error bars shown parallel to the ordinate axis represent the uncertainty in measuring the steady state pressure from the pressure traces created by the superposition of the high frequency noise on the pressure profile of birds. The error bars shown parallel to the abscissa are based on the maximum error in determining the initial impact location on the target. The maximum error was calculated in Reference 5 by Bauer and is

[6]Boehman, L.I. and A. Challita, "A Model for Predicting Bird and Ice Impact Loads on Structures," UDR-TR-79-54.

[5]Bauer, D.P. and J.P. Barber, "Experimental Investigation of Impact Pressures Caused by Gelatin Simulated Birds and Ice," UDR-TR-78-114, November 1978.

caused by the displacement of the actual trajectory from the true trajectory of the projectile.

This set of figures shows the important effect that impact angle has on steady flow distribution. As the impact angle changes from normal to oblique, the steady flow pressure distribution changes from symmetrical about the center of impact to highly skewed about the stagnation point. It also shows that the location of the stagnation point in the flow field moves from the center of impact to a point actually outside the projected frontal area of the incoming projectile. The figures show that projectile size has no effect on steady flow pressures. The data for both 1800 g and 3600 g gelatin projectiles are included in the figures and, in nondimensionalized (scaled) form, show no significant departure from the smaller bird results.

Agreement among the theoretical curve, curve fit of the experimental data for smaller size gelatin projectiles, and the experimental data from this work is very good at all angles of impact. Some disagreement between the data and the flow model predictions does occur near the outside edge of the flow, because the analytically predicted pressure distribution was generated from a simplified model of onset flow.

3.4.2 Real Birds

Figures 17, 18, and 19 show the steady flow pressure distributions along the major axis for real bird impacts. Again, the theory and the least-squares curve fit of the experimental data for smaller size birds from Reference 3 by Barber are shown on these figures. Error bars similar to that shown for gelatin are also shown.

All of the characteristics of steady flow apparent in the gelatin impacts are also apparent for real birds. The

---

[3]Barber, J.P., H.R. Taylor, and J.S. Wilbeck, "Bird Impact Forces and Pressures on Rigid and Compliant Targets," AFFDL-TR-77-60, ADA061-313, May 1978.

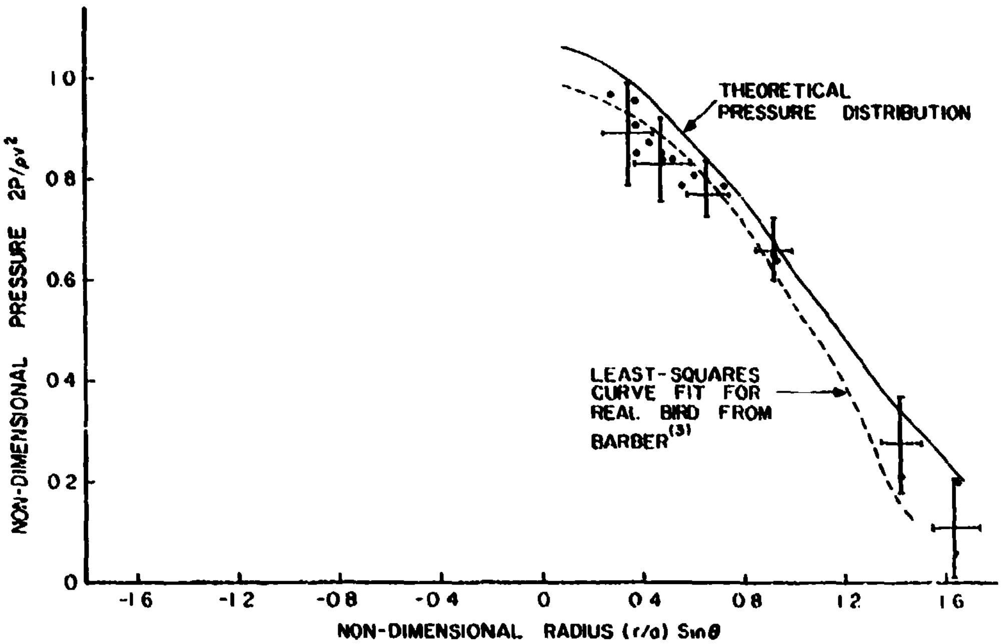

Figure 17. Normalized Steady Flow Pressure Distribution of Nominal 1800 g Real Bird (chicken) Along Major Axis at Normal Impact

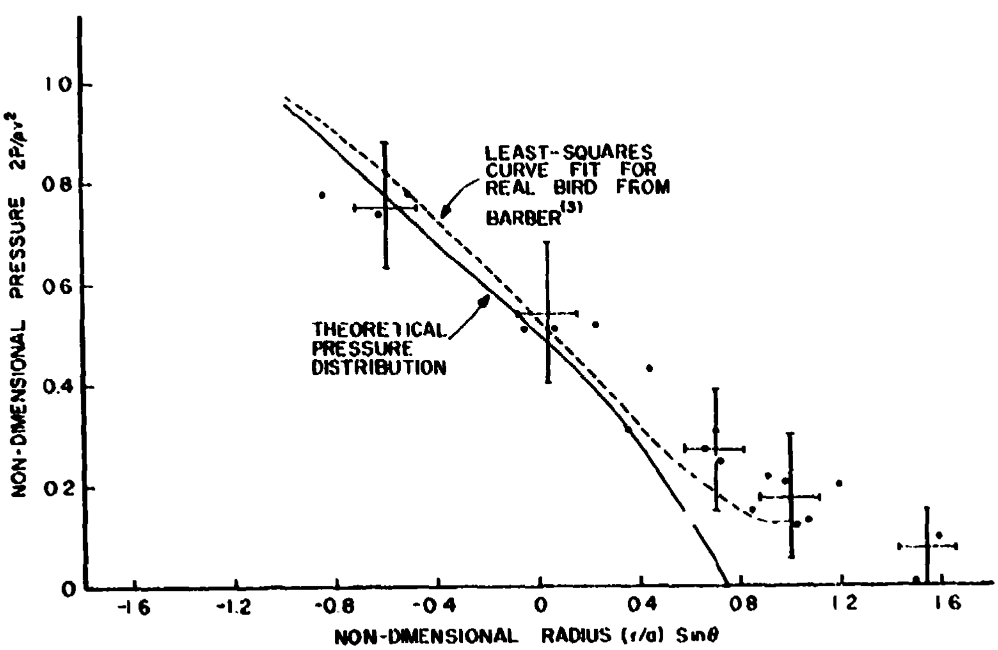

Figure 18. Normalized Steady Flow Pressure Distribution of Nominal 1800 g Real Bird (chicken) Along Major Axis at 45° Impact

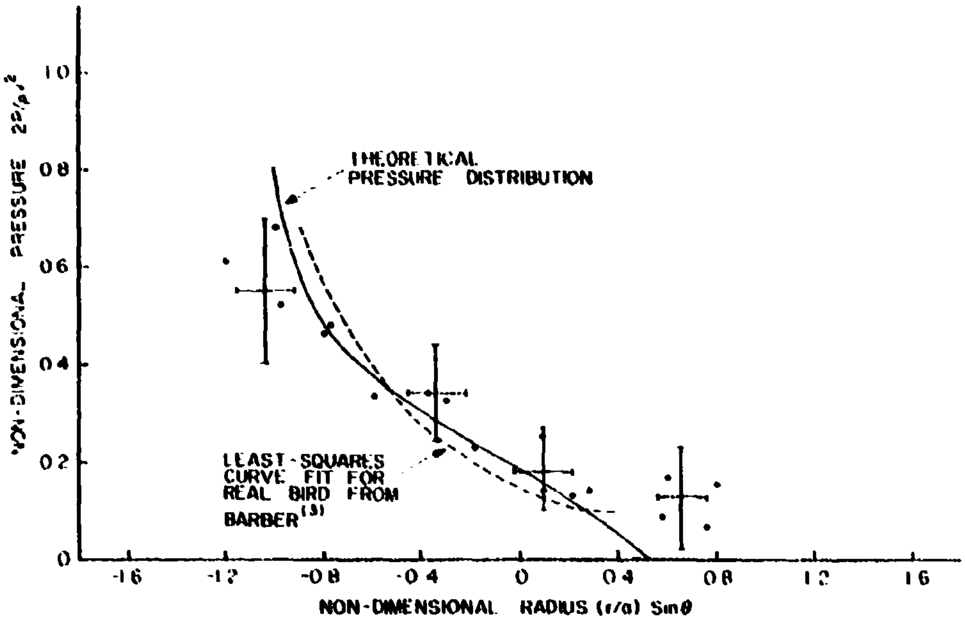

Figure 19. Normalized Steady Flow Pressure Distribution of Nominal 1800 g Real Bird (chicken) Along Major Axis at 25° Impact

stagnation point moves from the center of impact to a point outside the projected frontal area of the incoming projectile and the steady flow pressure distribution is highly dependent on the impact angle. There is good agreement among the theoretical curve, curve fit of the experimental data for smaller size birds, and the experimental data from this program.

This data also demonstrates that for the 1800 g projectiles, there are no significant differences between loads produced by real and gelatin birds. In Reference 5 Bauer found a similar result for 90 g and 600 g projectiles.

---

[5]Bauer, D.P. and J.P. Barber, "Experimental Investigation of Impact Pressures Caused by Gelatin Simulated Birds and Ice," UDR-TR-78-114, November 1978.

SECTION IV

CONCLUSIONS AND DISCUSSION

A detailed body of impact pressure data now exists for real birds (chickens) and bird substitutes (gelatin with 10 percent porosity) over an enormous range of impact parameters. The parameters and their ranges are:

1) Bird mass - 60 g to 3600 g
2) Impact velocity - 50 m/s to 300 m/s
3) Impact angle - 25° to 90°

This entire body of data has been successfully analysed and the important impact processes identified, functional relationships between the impact pressures and impact parameters developed and scaling of impact loads with bird mass completed. From the work reported here and in Reference 3 by Barber, Reference 2 by Peterson and Barber, Reference 4 by Wilbeck, and Reference 5 by Bauer, the following conclusions may be drawn.

1) Birds behave as a fluid during impact at the impact velocities of interest in birdstrike (>50 m/s).

---

[3]Barber, J.P., H.R. Taylor, and J.S. Wilbeck, "Bird Impact Forces and Pressures on Rigid and Compliant Targets," AFFDL-TR-77-60, ADA061-313, May 1978.

[2]Peterson, R.L. and J.P. Barber, "Bird Impact Forces in Aircraft Windshield Design," AFFDL-TR-75-150, ADA026-628, March 1976.

[4]Wilbeck, J.S., "Impact Behavior of Low Strength Projectiles," AFML-TR-77-134, ADA060-423, July 1978.

[5]Bauer, D.P. and J.P. Barber, "Experimental Investigation of Impact Pressures Caused by Gelatin Simulated Birds and Ice," UDR-TR-78-114, November 1978.

2) There are four phases of fluid behavior during a bird impact; the shock phase of initial impact, shock pressure decay, steady flow, and termination.

3) Peak shock pressures are independent of bird mass but depend in a predictable manner on impact velocity, impact angle, and bird material properties.

4) Steady flow pressures are independent of bird mass but depend in a predictable way on impact velocity, impact angle, and bird material properties.

5) The spacial distribution of bird impact pressures scale linearly with bird dimensions (providing bird orientation at impact is fixed). This scaling has been tested over a range of bird mass from 60 g to 3600 g.

6) Impact duration is given by simply the length of the bird divided by the impact velocity. The validity of this relation has been tested for bird masses from 60 to 3600 g and for impact velocities from 50 m/s to 300 m/s.

7) Simulated birds effectively reproduce the pressure distribution of real birds.

APPENDIX
BIRD LOADING MODEL

This appendix provides a listing of the modified bird loading model, a sample input and output data, and the instructions needed to run the program.

The original loading model was designed to predict impact loads and to be interfaced with finite element structural analysis computer programs, and also was designed to handle impacts on arbitrary curved surfaces. The three-dimensional potential flow theory was used to model the impact process and the surface singularity method was used to solve the complex potential flows (i.e., velocity and pressure fields). To allow arbitrary bodies to be considered, it was required that the body surface be specified by a set of points in space called nodal points and that the coordinates of all nodal points on the impacted surface be supplied to the loading model.

Input to the loading model consisted of the coordinates of the set of finite element nodal points defining the surface of the impacted object. These coordinates were given in the reference coordinate system, that is, the coordinate system used to describe the shape of the impacted surface before impact occurs.

Because the target used in this experimental program is a rigid flat plate, the loading model was modified to generate a rectangular grid describing the plate. The dimensions of the grid are proportional to the weight of the bird and to the angle of impact. The number of elements forming the grid is found by multiplying NC by NS, where NC and NS are the number of nodes along the width and length of the grid.

The input data needed for this modified version of the loading model are time, TIM, which is assumed to equal zero;

components of the velocity vector of the projectile, VBX, VBY, and VBZ; coordinates of the center of impact, XI, YI, and ZI; angle of impact, THETA; and the weight of the projectile, WB. The bird length is assumed to be twice its diameter.

The output data are divided in two parts; the first part lists the coordinates of the four corner points forming the element, the components of the unit normal vector, and the coordinates of the null point in the reference coordinate system. The main purpose of this output is to enable errors in the input to be discovered before the lengthy flow calculations are performed. The second part contains the velocities and pressures on the body surface.

Listing of the Main Program

```
      PROGRAM FOAMPR(INPUT,OUTPUT,TAPE5,TAPE11)
C
C     THIS PROGRAM CALCULATES THE POTENTIAL FLOW ABOUT ARBITRARY,
C     THREE-DIMENSIONAL BODIES. PLANE QUADRILATERAL SURFACE ELEMENTS
C     ARE USED TO APPROXIMATE THE BODY SURFACE. THE METHOD SELECTS
C     A SOURCE DENSITY DISTRIBUTION ON THE SURFACE OF THE BODY AND SOLVE
C     FOR THE DISTRIBUTION NECESSARY TO MAKE THE NORMAL VELOCITY
C     ZERO ON THE BOUNDARY. THE INTEGRAL EQUATION FOR THE SURFACE
C     SOURCE DENSITY IS REPLACED BY A SET OF LINEAR ALGEBRAIC
C     EQUATIONS FOR THE VALUES OF THE SOURCE DENSITY ON EACH OF THE
C     QUADRILATERAL ELEMENTS. AFTER THIS SET OF EQUATIONS HAS BEEN
C     SOLVED,WHICH IS ACCOMPLISHED BY A SIMPLE ITERATIVE PROCEDURE,
C     THE FLOW VELOCITIES AT POINTS ON THE BODY SURFACE ARE CALCULATED.
C
      DIMENSION A(3,121),VX(121,121),VY(121,121),VZ(121,121)
     1          ,AN(121,121),ON(121),S(121),X(4,121),Y(4,121),
     2           Z(4,121),P(121),XN(121),YN(121),ZN(121),UX(121),
     3           UY(121),UZ(121),JON(121),T(3,3,121)
      REAL M12,M23,M34,M41
      PI=3.14159
      READ (5,901) TTM,VRX,VRY,VRZ,XI,YI,ZI
      WRITE (11,902)
      WRITE (11,903) TTM,VRX,VRY,VRZ,XI,YI,ZI
      READ (5,904) THETA,WB
      THETA=THETA*PI/180.
      NC=11
      NS=11
      WRITE (11,905)
      WRITE (11,906) THETA,WB
      RHOB=.03644
      VR=(VRX**2+VRY**2+VRZ**2)**0.5
      DB=(2.*WB/(PI*RHOB))**.3333
      RB=2.*DB
      RI=DB/2.
      RIP=RI/SIN(THETA)
      ELINC=RIP/5.
      GREEN=RIP
      SUM1=1.
      DO 9 J=1,NS
      SUM=0.
      DO 8 I=1,NC
      II=NC*(J-1)+I
      XN(II)=GREEN-SUM*ELINC
      YN(II)=-GREEN+SUM1*ELINC
      SUM=SUM+1.
    8 CONTINUE
      SUM1=SUM1+1.
    9 CONTINUE
      COSAL=VRX/VR
      COSBE=VRY/VR
```

```
      [illegible]
      WRITE (11,808)
      WRITE (11,903) [illegible]
  901 FORMAT([illegible])
  904 FORMAT([illegible])
  902 FORMAT (' ',2X,'TIME',2X,[illegible]
     1 [illegible])
  903 FORMAT (F10.4)
  905 FORMAT ([illegible])
  906 FORMAT (F10.4)
  907 FORMAT (F10.4)
  808 FORMAT ([illegible])
  908 FORMAT (9F8.3)
      WRITE (11,909)
  909 FORMAT (' X COORDS. OF NULL POINTS')
      WRITE (11,700) (XN(I),I=1,12)
  700 FORMAT (10(2X,F10.3))
      WRITE (11,701)
  701 FORMAT (' Y COORDS. OF NULL POINTS')
      WRITE (11,700) (YN(I),I=1,12)
  702 FORMAT (' Z COORDS. OF NULL POINTS')
      IR=NC*NS
      N=IR
      DO 7 I=1,IR
      ZN(I)=0.
      UX(I)=0.
      UY(I)=0.
      UZ(I)=0.
    7 CONTINUE
      WRITE (11,702)
      WRITE (11,700) (ZN(I),I=1,12)
      LL=1
      KK=1
      DO 800 I=1,IR
  205 MM=I-(KK-1)*NC
      IF (MM.LE.NC) GO TO 210
      KK=KK+1
      GO TO 205
  210 IF (MM.NE.1) GO TO 250
      LK=I+NC
      IF (KK.EQ.1) GO TO 220
      LM=I-NC
      X(1,I)=X(4,LM)
      Y(1,I)=Y(4,LM)
      Z(1,I)=Z(4,LM)
      X(2,I)=X(3,LM)
      Y(2,I)=Y(3,LM)
      Z(2,I)=Z(3,LM)
      IF (KK.EQ.NS) GO TO 230
  220 X(4,I)=(XN(K)+XN(L))/2.
```

```
      Y(4,1)=(YN(K)+YN(I))/2.
      Z(4,1)=(ZN(K)+ZN(I))/2.
      JM=K+1
      X(3,1)=(XN(JM)+XN(I))/2.
      Y(3,1)=(YN(JM)+YN(I))/2.
      Z(3,1)=(ZN(JM)+ZN(I))/2.
      IF(KK.EQ.1) GO TO 240
      GO TO 800
  240 X(4,1)=XN(I)+(XN(I)-XN(M))/2.
      Y(4,1)=YN(I)+(YN(I)-YN(M))/2.
      Z(4,1)=ZN(I)+(ZN(I)-ZN(M))/2.
      Z(3,1)=(Z(4,1)+(ZN(I+1)+(ZN(I+1)-ZN(M+1))/2.))/2.
      Y(3,1)=(Y(4,1)+(YN(I+1)+(YN(I+1)-YN(M+1))/2.))/2.
      X(3,1)=(X(4,1)+(XN(I+1)+(XN(I+1)-XN(M+1))/2.))/2.
      GO TO 800
  245 X(1,1)=XN(I)+(XN(K)-XN(I))/2.
      Y(1,1)=YN(I)+(YN(K)-YN(I))/2.
      Z(1,1)=ZN(I)+(ZN(K)-ZN(I))/2.
      Z(2,1)=(Z(1,1)+(ZN(I+1)+(ZN(K+1)-ZN(I+1))/2.))/2.
      Y(2,1)=(Y(1,1)+(YN(I+1)+(YN(K+1)-YN(I+1))/2.))/2.
      X(2,1)=(X(1,1)+(XN(I+1)+(XN(K+1)-XN(I+1))/2.))/2.
      GO TO 800
  250 IK=I+INC+1
      IM=I-NP
      JM=I-1
  252 X(4,1)=X(3,JM)
      Y(4,1)=Y(3,JM)
      Z(4,1)=Z(3,JM)
      IF(KK.EQ.1) GO TO 260
  254 X(1,1)=X(4,IM)
      Y(1,1)=Y(4,IM)
      Z(1,1)=Z(4,IM)
  256 X(2,1)=X(3,IM)
      Y(2,1)=Y(3,IM)
      Z(2,1)=Z(3,IM)
      IF(KK.EQ.NS) GO TO 265
      IF(MM.EQ.NC) GO TO 265
  262 X(3,1)=(XN(I)+XN(IK))/2.
      Y(3,1)=(YN(I)+YN(IK))/2.
      Z(3,1)=(ZN(I)+ZN(IK))/2.
      GO TO 800
  260 X(1,1)=X(2,I-1)
      Y(1,1)=Y(2,I-1)
      Z(1,1)=Z(2,I-1)
      IK=I+INC
      X(2,1)=XN(I)+(XN(I+INC+1)-XN(I))/2.
      Y(2,1)=YN(I)+(YN(I+INC+1)-YN(I))/2.
      Z(2,1)=ZN(I)+(ZN(I+INC+1)-ZN(I))/2.
      IF(KK.EQ.1.AND.MM.NE.NC) GO TO [illegible]
  265 Z(3,1)=ZN(I)+(ZN(I)-Z(1,1))
```

```
      Y(3,I)=YN(I)+(YN(I)-Y(1,I))
      X(3,I)=XN(I)+(XN(I)-X(1,I))
  800 CONTINUE
   14 WRITE (11,1)
    1 FORMAT (*0*,* J=ELEMENT NUMBER*)
      WRITE (11,2)
    2 FORMAT (* *,* X1,X2,X3,X4 X COORDINATES OF THE POINTS FORMING*,
     1 * THE ELEMENTS*)
      WRITE (11,3)
    3 FORMAT (* *,* Y1,Y2,Y3,Y4 Y COORDINATES OF THE POINTS FORMING*,
     1 * THE ELEMENTS*)
      WRITE (11,4)
    4 FORMAT (* *,* Z1,Z2,Z3,Z4 Z COORDINATES OF THE POINTS FORMING*,
     1 * THE ELEMENTS*)
      WRITE (11,5)
    5 FORMAT (* *,* UNX,UNY,UNZ=COMPONENTS OF THE UNIT NORMAL VECTOR*)
      WRITE (11,6)
    6 FORMAT (* *,* XPNP,YPNP,ZPNP=COORDINATES OF THE NULL POINT IN*,
     1 * REFERENCE COORDINATE SYSTEM*)
      WRITE (11,85)
   85 FORMAT (//3X,*J*,7X,*X1*,7X,*X2*,7X,*X3*,7X,*X4*,6X,*UNX*,6X,
     1 *XPNP*)
      WRITE (11,1085)
 1085 FORMAT (11X,*Y1*,7X,*Y2*,7X,*Y3*,7X,*Y4*,6X,*UNY*,6X,*YPNP*)
      WRITE (11,87)
   87 FORMAT (11X,*Z1*,7X,*Z2*,7X,*Z3*,7X,*Z4*,6X,*UNZ*,6X,*ZPNP*/)
  151 DO 10 J=1,N
      X1=X(1,J)
      X2=X(2,J)
      X3=X(3,J)
      X4=X(4,J)
      Y1=Y(1,J)
      Y2=Y(2,J)
      Y3=Y(3,J)
      Y4=Y(4,J)
      Z1=Z(1,J)
      Z2=Z(2,J)
      Z3=Z(3,J)
      Z4=Z(4,J)
      T1X=X3-X1
      T1Y=Y3-Y1
      T1Z=Z3-Z1
      T2X=X4-X2
      T2Y=Y4-Y2
      T2Z=Z4-Z2
      XN1=T2Y*T1Z-T1Y*T2Z
      YN1=T1X*T2Z-T2X*T1Z
      ZN1=T2X*T1Y-T1X*T2Y
      UN=SQRT(XN1**2+YN1**2+ZN1**2)
      UNX=XN1/UN
```

```
UNY=YN1/UN
UNZ=ZN1/UN
XAV=(X1+X2+X3+X4)/4.
YAV=(Y1+Y2+Y3+Y4)/4.
ZAV=(Z1+Z2+Z3+Z4)/4.
D1=UNX*(XAV-X1)+UNY*(YAV-Y1)+UNZ*(ZAV-Z1)
D2=UNX*(XAV-X2)+UNY*(YAV-Y2)+UNZ*(ZAV-Z2)
D3=UNX*(XAV-X3)+UNY*(YAV-Y3)+UNZ*(ZAV-Z3)
D4=UNX*(XAV-X4)+UNY*(YAV-Y4)+UNZ*(ZAV-Z4)
XP1=X1+(UNX*D1)
XP2=X2+(UNX*D2)
XP3=X3+(UNX*D3)
XP4=X4+(UNX*D4)
YP1=Y1+(UNY*D1)
YP2=Y2+(UNY*D2)
YP3=Y3+(UNY*D3)
YP4=Y4+(UNY*D4)
ZP1=Z1+(UNZ*D1)
ZP2=Z2+(UNZ*D2)
ZP3=Z3+(UNZ*D3)
ZP4=Z4+(UNZ*D4)
TT=SQRT(TTX**2+TTY**2+TTZ**2)
TP1X=TTX/TT
TP1Y=TTY/TT
TP1Z=TTZ/TT
TP2X=UNY*TP1Z-UNZ*TP1Y
TP2Y=UNZ*TP1X-UNX*TP1Z
TP2Z=UNX*TP1Y-UNY*TP1X
ZETAP1=TP1X*(X1-XAV)+TP1Y*(Y1-YAV)+TP1Z*(Z1-ZAV)
ZETAP2=TP1X*(X2-XAV)+TP1Y*(Y2-YAV)+TP1Z*(Z2-ZAV)
ZETAP3=TP1X*(X3-XAV)+TP1Y*(Y3-YAV)+TP1Z*(Z3-ZAV)
ZETAP4=TP1X*(X4-XAV)+TP1Y*(Y4-YAV)+TP1Z*(Z4-ZAV)
ETAP1=TP2X*(X1-XAV)+TP2Y*(Y1-YAV)+TP2Z*(Z1-ZAV)
ETAP2=TP2X*(X2-XAV)+TP2Y*(Y2-YAV)+TP2Z*(Z2-ZAV)
ETAP3=TP2X*(X3-XAV)+TP2Y*(Y3-YAV)+TP2Z*(Z3-ZAV)
ETAP4=TP2X*(X4-XAV)+TP2Y*(Y4-YAV)+TP2Z*(Z4-ZAV)
ZETAOR=(1./(3.*(ETAP2-ETAP4)))*(ZETAP4*(ETAP1-ETAP2)+ZETAP2*(ETAP4
1     -ETAP1))
ETAOR=-1./3.*ETAP1
ZETA1=ZETAP1-ZETAOR
ZETA2=ZETAP2-ZETAOR
ZETA3=ZETAP3-ZETAOR
ZETA4=ZETAP4-ZETAOR
ETA1=ETAP1-ETAOR
ETA2=ETAP2-ETAOR
ETA3=ETAP3-ETAOR
ETA4=ETAP4-ETAOR
XO=XAV+TP1X*ZETAOR+TP2X*ETAOR
YO=YAV+TP1Y*ZETAOR+TP2Y*ETAOR
ZO=ZAV+ZETAOR*TP1Z+TP2Z*ETAOR
```

```
251.0000        ?(1,1)=X0
252.0000        ?(2,1) YO
253.0000        ?(3,1)=ZO
254.0000        1(1,1,1)=HP1X
255.0000        1(1,2,1)=HP1Y
256.0000        1(1,3,1) HP1Z
257.0000        1(2,1,1)=HP2X
258.0000        1(2,2,1)=HP2Y
259.0000        1(2,3,1)=HP2Z
260.0000        1(3,1,1)=HNX
261.0000        1(3,2,1)=HNY
262.0000        1(3,3,1) HNZ
263.0000        XX=0.
264.0000        YY 0.
265.0000        ZZ=0.
266.0000 80     [illegible]
267.0000        [illegible]
268.0000        [illegible]
269.0000        [illegible]
270.0000        R1 SQRT((XX [illegible]
271.0000        R2 SQRT((XX [illegible]
272.0000        R3=SQRT((XX [illegible]
273.0000        R4=SQRT((XX [illegible]
274.0000        [illegible] /R23
275.0000        [illegible] /R12
276.0000        [illegible] /R34
277.0000        [illegible] /R41
278.0000        XO1 [illegible]
279.0000        [illegible]
280.0000        [illegible]
281.0000        [illegible]
282.0000        [illegible]
283.0000        YO1 [illegible]
284.0000        IF (ABS(XO1).LT.0.0001.AND.ABS(YO1).LT.0.0001) GO TO 50
285.0000        R1R2X=(XX [illegible] /R2
286.0000        R2R3X=(XX [illegible] /R3
287.0000        R3R4X [illegible] /R4
288.0000        R4R1X [illegible] /R1
289.0000        R1R2Y [illegible] /R2
290.0000        R2R3Y [illegible] /R3
291.0000        R3R4Y=(YY [illegible] /R4
292.0000        R4R1Y=(YY [illegible] /R1
293.0000        DD12 [illegible] /2.
294.0000        DD23 [illegible] /2.
295.0000        DD34 [illegible] /2.
296.0000        DD41 [illegible] /2.
297.0000        VXX (ETA2 ETA1)*R1R2X [illegible] (ETA3 ETA2)*R2R3X/DD23
298.0000        VXX=VXX+((ETA4 ETA3)*R3R4X/DD34+((ETA1 ETA4)*R4R1X/DD41
299.0000        VXY=((ETA2 ETA1)*R1R2Y/DD12 [illegible] (ETA3 ETA2)*R2R3Y/DD23
300.0000        VXY=VXY+((ETA4-ETA3)*R3R4Y/DD34+((ETA1-ETA4)*R4R1Y/DD41
```

```
      UYX=(ZETA1-ZETA2)*RK*[illegible]*RAX/UHE3
      UYX=UYX+(ZETA3-ZETA4)*RK*RAX/UHE[illegible](ZETA4-ZETA1)*RK*RAX/UHE4
      UYY=(ETA1-ETA2)*RK*[illegible]*RAY/UHE3
      UYY=UYY+(ETA3-ETA4)*RK*RAY/UHE[illegible](ETA4-ETA1)*RK*RAY/UHE4
      UE1=UXX*UYY-UYX*UXY
      UELX=(-UEE*UYY+UYE*UXY)/UE1
      UELY=(UXX*YUE-UYX*XUE)/UE1
      XX=XX+UELX
      YY=YY+UELY
      GO TO 80
   90 CONTINUE
      XPNP=XUE+TP1*XX+TP2X*YY
      YPNP=YUE+TP1Y*XX+TP2Y*YY
      ZPNP=ZUE+TP1Z*XX+TP2Z*YY
      A(1,J)=XPNP
      A(2,J)=YPNP
      A(3,J)=ZPNP
      X(1,J)=ZETA1
      X(2,J)=ZETA2
      X(3,J)=ZETA3
      X(4,J)=ZETA4
      X(4,J)=ZETA4
      Y(1,J)=ETA1
      Y(2,J)=ETA2
      Y(3,J)=ETA3
      Y(4,J)=ETA4
      WRITE (11,100) J,X1,X2,X3,X4,UNX,XPNP
  100 FORMAT (I4,6F10.5)
      WRITE (11,110) Y1,Y2,Y3,Y4,UNY,YPNP
  110 FORMAT (4X,6F10.5)
      WRITE (11,111) Z1,Z2,Z3,Z4,UNZ,ZPNP
  111 FORMAT (4X,6F10.5/)
   10 CONTINUE
      II=1
  132 IF (II .EQ. 1) NN=N
      DO 617 J=1,N
      ELX1=E(1,1,J)*(X1-Z(1,J))+E(1,2,J)*(Y1-Z(2,J))
      ELX1=ELX1+E(1,3,J)*(Z1-Z(3,J))
      ELY1=E(2,1,J)*(X1-Z(1,J))+E(2,2,J)*(Y1-Z(2,J))
      ELY1=ELY1+E(2,3,J)*(Z1-Z(3,J))
      ELZ1=E(3,1,J)*(X1-Z(1,J))+E(3,2,J)*(Y1-Z(2,J))
      ELZ1=ELZ1+E(3,3,J)*(Z1-Z(3,J))
      ELURX=E(1,1,J)*URX+E(1,2,J)*URY+E(1,3,J)*URZ
      ELURY=E(2,1,J)*URX+E(2,2,J)*URY+E(2,3,J)*URZ
      ELURZ=E(3,1,J)*URX+E(3,2,J)*URY+E(3,3,J)*URZ
      ELUR=(ELURX**2+ELURY**2+ELURZ**2)**0.5
      COSA=ELURX/ELUR
      COSB=ELURY/ELUR
      COSG=ELURZ/ELUR
      XINT=ELX1-(ELZ1*COSA/COSG)
```

```
      YINT=ELYI-(ELZI*COSB/COSG)
      DISX=COSG*YINT
      DISY=COSB*YINT
      DISZ=COSB*YINT-COSA*YINT
      DIST=(DISX**2+DISY**2+DISZ**2)**.5
      IF(DIST.GT.RE) JON(J)=0
      IF(DIST.LT.RE) JON(J)=1
      D1=(X(2,J)-X(1,J))**2+(Y(2,J)-Y(1,J))**2
      D2=(X(4,J)-X(3,J))**2+(Y(4,J)-Y(3,J))**2
      D3=(X(3,J)-X(2,J))**2+(Y(3,J)-Y(2,J))**2
      D4=(X(4,J)-X(1,J))**2+(Y(4,J)-Y(1,J))**2
      D5=(X(1,J)-XINT)**2+(Y(1,J)-YINT)**2
      D6=(X(4,J)-XINT)**2+(Y(4,J)-YINT)**2
      D7=(X(3,J)-XINT)**2+(Y(3,J)-YINT)**2
      D8=(X(2,J)-XINT)**2+(Y(2,J)-YINT)**2
      G1=(D7+D8-D3)/(2.*SQRT(D7)*SQRT(D8))
      IF (G1.LT.0.) GO TO 610
      IF (G1.GT.1..AND.G1.LT.1.01) G1=1.
      GO TO 611
610   IF (G1.LT.-1..AND.G1.GT.-1.01) G1=-1.
611   ANG1=ACOS(G1)
      G2=(D6+D7-D2)/(2.*SQRT(D6)*SQRT(D7))
      IF (G2.LT.0.) GO TO 612
      IF (G2.GT.1..AND.G2.LT.1.01) G2=1.
      GO TO 613
612   IF (G2.LT.-1..AND.G2.GT.-1.01) G2=-1.
613   ANG2=ACOS(G2)
      G3=(D5+D6-D4)/(2.*SQRT(D5)*SQRT(D6))
      IF (G3.LT.0.) GO TO 614
      IF (G3.GT.1..AND.G3.LT.1.01) G3=1.
      GO TO 615
614   IF (G3.LT.-1..AND.G3.GT.-1.01) G3=-1.
615   ANG3=ACOS(G3)
      G4=(D5+D8-D1)/(2.*SQRT(D5)*SQRT(D8))
      IF (G4.LT.0.) GO TO 616
      IF (G4.GT.1..AND.G4.LT.1.01) G4=1.
      GO TO 617
616   IF (G4.LT.-1..AND.G4.GT.-1.01) G4=-1.
617   ANG4=ACOS(G4)
      ANG=ANG1+ANG2+ANG3+ANG4
      IF (ABS(ANG).LT.6.27) GO TO 627
      IMP=J
      WRITE(11,230) IMP
230   FORMAT(2X,'IMPACT POINT IS ON ELEMENT',I5)
627   CONTINUE
622   UXRR=VRX-UX(IMP)
      UYRR=VRY-UY(IMP)
      UZRR=VRZ-UZ(IMP)
      VRR2=UXRR**2+UYRR**2+UZRR**2
      VRR=SQRT(VRR2)
```

```
      IF (TIM.NE.0.) GO TO 13
      TERM=DL/VBR
      XLC=0.
      GO TO 22
 13   DLC=VBR*(TIM-TINIT)
      TINIT=0.
      XLC=XLC+DLC
      DLR=DL-XLC
      TERM=TIM+DLR/VBR
 22   PDYN=0.5*RHO*VBR2
      DO 1001 I=1,IB
      DX(I)=DX(I)/VBR
      DY(I)=DY(I)/VBR
      DZ(I)=DZ(I)/VBR
 1001 CONTINUE
      DO 15 I=1,NN
      U1=0.
      V1=0.
      W1=0.
  167 X1=A(1,I)
      Y1=A(2,I)
      Z1=A(3,I)
  136 DO 20 J=1,N
      XNP=T(1,1,J)*(X1-Z(1,J))+T(1,2,J)*(Y1-Z(2,J))+T(1,3,J)*(Z1-Z(3,J))
      YNP=T(2,1,J)*(X1-Z(1,J))+T(2,2,J)*(Y1-Z(2,J))+T(2,3,J)*(Z1-Z(3,J))
      ZNP=T(3,1,J)*(X1-Z(1,J))+T(3,2,J)*(Y1-Z(2,J))+T(3,3,J)*(Z1-Z(3,J))
      ZL21=X(2,J)-X(1,J)
      ZL32=X(3,J)-X(2,J)
      ZL43=X(4,J)-X(3,J)
      ZL14=X(1,J)-X(4,J)
      ET21=Y(2,J)-Y(1,J)
      ET32=Y(3,J)-Y(2,J)
      ET43=Y(4,J)-Y(3,J)
      ET14=Y(1,J)-Y(4,J)
      D12=SQRT(ZL21**2+ET21**2)
      D23=SQRT(ZL32**2+ET32**2)
      D34=SQRT(ZL43**2+ET43**2)
      D41=SQRT(ZL14**2+ET14**2)
      R1=SQRT((XNP-X(1,J))**2+(YNP-Y(1,J))**2+ZNP**2)
      R2=SQRT((XNP-X(2,J))**2+(YNP-Y(2,J))**2+ZNP**2)
      R3=SQRT((XNP-X(3,J))**2+(YNP-Y(3,J))**2+ZNP**2)
      R4=SQRT((XNP-X(4,J))**2+(YNP-Y(4,J))**2+ZNP**2)
      E1=ZNP**2+(XNP-X(1,J))**2
      E2=ZNP**2+(XNP-X(2,J))**2
      E3=ZNP**2+(XNP-X(3,J))**2
      E4=ZNP**2+(XNP-X(4,J))**2
      H1=(YNP-Y(1,J))*(XNP-X(1,J))
      H2=(YNP-Y(2,J))*(XNP-X(2,J))
      H3=(YNP-Y(3,J))*(XNP-X(3,J))
      H4=(YNP-Y(4,J))*(XNP-X(4,J))
```

```
      U11=ALOG((R1+R2-D12)/(R1+R2+D12))*E12/D12
      U22=ALOG((R2+R3-D23)/(R2+R3+D23))*E23/D23
      U33=ALOG((R3+R4-D34)/(R3+R4+D34))*E43/D34
      U44=ALOG((R4+R1-D41)/(R4+R1+D41))*E14/D41
      XUT=U11+U22+U33+U44
      V11=ALOG((R1+R2-D12)/(R1+R2+D12))*(-ZE21/D12)
      V22=ALOG((R2+R3-D23)/(R2+R3+D23))*(-ZE32/D23)
      V33=ALOG((R3+R4-D34)/(R3+R4+D34))*(-ZE43/D34)
      V44=ALOG((R4+R1-D41)/(R4+R1+D41))*(-ZE14/D41)
      YUT=V11+V22+V33+V44
      DIA1=SQRT((X(3,I)-X(1,I))**2+(Y(3,I)-Y(1,I))**2)
      DIA2=SQRT((X(4,I)-X(2,I))**2+(Y(4,I)-Y(2,I))**2)
      IF(DIA2 .GT. DIA1) DIA1=DIA2
      DIA1=DIA1/50.
      IF(ABS(ZNP) .GT. ABS(DIA1)) GO TO 40
      IF(I .EQ. J) ZW1=2.*PI
      IF(I .NE. J) ZW1=0.
      GO TO 30
   40 IF(ZE21 .EQ. 0.)  W11=0.
      IF(ZE21 .EQ. 0.)   GO TO 42
      M12=E21/ZE21
      W11=ATAN2((M12*E1-H1),(ZNP*R1))-ATAN2((M12*E2-H2),(ZNP*R2))
   42 IF(ZE32 .EQ. 0.)   W22=0.
      IF(ZE32 .EQ. 0.)   GO TO 44
      M23=E32/ZE32
      W22=ATAN2((M23*E2-H2),(ZNP*R2))-ATAN2((M23*E3-H3),(ZNP*R3))
   44 IF(ZE43 .EQ. 0.)  W33=0.
      IF(ZE43 .EQ. 0.)   GO TO 46
      M34=E43/ZE43
      W33=ATAN2((M34*E3-H3),(ZNP*R3))-ATAN2((M34*E4-H4),(ZNP*R4))
   46 IF(ZE14 .EQ. 0.)   W44=0.
      IF(ZE14 .EQ. 0.)   GO TO 35
      M41=E14/ZE14
      W44=ATAN2((M41*E4-H4),(ZNP*R4))-ATAN2((M41*E1-H1),(ZNP*R1))
   35 ZW1=W11+W22+W33+W44
   30 UPX=T(1,1,I)*XUT+T(2,1,I)*YUT+T(3,1,I)*ZW1
      VPY=T(1,2,I)*XUT+T(2,2,I)*YUT+T(3,2,I)*ZW1
      WPZ=T(1,3,I)*XUT+T(2,3,I)*YUT+T(3,3,I)*ZW1
  141 UX(I,J)=UPX
      UY(I,J)=VPY
      UZ(I,J)=WPZ
      AN(I,J)=T(3,1,I)*UPX+T(3,2,I)*VPY+T(3,3,I)*WPZ
   20 CONTINUE
      IF(ION(I) .EQ. 0)   GO TO 109
      VINFX=COSAL-UX(I)
      VINFY=COSAB-UY(I)
      VINFZ=COSGA-UZ(I)
      UN(I)=-(T(3,1,I)*VINFX+T(3,2,I)*VINFY+T(3,3,I)*VINFZ)
      GO TO 15
  109 UN(I)=0.
```

```
 15   CONTINUE
      CALL SEIDEL (AN,BN,S,N)
      WRITE (11,92)
  92  FORMAT (2X,*I*,7X,*XPNP*,9X,*VEL*,10X,*U1*,9X,*UNX*)
      WRITE (11,93)
  93  FORMAT (10X,*YPNP*,8X,*SQVEL*,9X,*V1*,9X,*UNY*)
      WRITE (11,94)
  94  FORMAT (10X,*ZPNP*,10X,*CP*,10X,*W1*,9X,*UNZ*/)
      DO 101 I=1,N
      U1=0.
      V1=0.
      W1=0.
      DO 102 J=1,N
      T1=VX(I,J)*S(J)
      T2=VY(I,J)*S(J)
      T3=VZ(I,J)*S(J)
      U1=U1+T1
      V1=V1+T2
      W1=W1+T3
 102  CONTINUE
      IF(BN(I) .EQ. 0.) GO TO 310
      U1=U1+COSAL-UX(I)
      V1=V1+COSBE-UY(I)
      W1=W1+COSGA-UZ(I)
 310  CONTINUE
      VEL=SQRT(U1**2+V1**2+W1**2)
      SQVEL=VEL**2
      CP=1.-SQVEL
      P(I)=CP*PDYN
      IF(ABS(A(1,I)) .GE. .5) GO TO 101
      WRITE (11,103) I,A(1,I),VEL,U1,T(3,1,I)
 103  FORMAT (I4,4F12.4)
      WRITE (11,104) A(2,I),SQVEL,V1,T(3,2,I)
 104  FORMAT (4X,4F12.4)
      WRITE (11,105) A(3,I),CP,W1,T(3,3,I)
 105  FORMAT (4X,4F12.4/)
 101  CONTINUE
      TINIT=TIM
      WRITE (11,926)
  926 FORMAT (//,* PRESSURES AT THE NULL POINTS*)
      WRITE (11,927) (P(I),I=1,121)
  927 FORMAT (10(2X,F10.2))
      STOP
      END
      SUBROUTINE SEIDEL (A,B,X,N)
C
C      ITERATIVE SOLUTION OF A SET OF SIMULTANEOUS
C      LINEAR EQUATIONS USING THE GAUSS-SEIDEL METHOD
C
       DIMENSION A(N,N),B(N),X(N),BMAT(175,175),C(175),XOLD(175)
```

```
      DO 10 I=1,N
      X(I)=0.
10    CONTINUE
      TOL=1.E-4
      WRITE (11,15)
15    FORMAT (/* VALUES OF 1ST AND LAST X-ELEMENTS 0*)
      DO 30 I=1,N
      IF (ABS(A(I,I)).LT.1.E-30) GO TO 40
      DO 20 J=1,N
      BMAT(I,J)=-A(I,J)/A(I,I)
      IF (I.EQ.J) BMAT(I,J)=0.
20    CONTINUE
      C(I)=B(I)/A(I,I)
30    CONTINUE
      GO TO 55
40    WRITE (11,50) I
50    FORMAT (*0*,*DIAGONAL COEFFICIENT NO.*,I3,* =0.*)
      STOP
55    DO 110 M=1,500
      DO 90 I=1,N
      XOLD(I)=X(I)
      SUM1=0.
      SUM2=0.
      IF (I.EQ.1) GO TO 70
      I1=I-1
      DO 60 J=1,I1
      SUM1=SUM1+BMAT(I,J)*X(J)
60    CONTINUE
70    I2=I+1
      IF (I2.GT.N) GO TO 85
      DO 80 J=I2,N
      SUM2=SUM2+BMAT(I,J)*X(J)
80    CONTINUE
85    X(I)=SUM1+SUM2+C(I)
90    CONTINUE
      WRITE (11,95) X(1),X(N)
95    FORMAT (2E12.5)
      RMAX=0.
      DO 100 I=1,N
      R=X(I)-XOLD(I)
      IF (R.LT.TOL) GO TO 100
      RREL=ABS(R/X(I))
      RMAX=AMAX1(RMAX,RREL)
100   CONTINUE
      IF (RMAX.LT.TOL) GO TO 130
110   CONTINUE
      WRITE (11,120)
120   FORMAT (*0*,*DID NOT CONVERGE IN 500 ITERATIONS*)
      STOP
130   RETURN
      END
```

Sample of Input Data

```
0.,0.,297.,-138.,0.,0.,0.,
25.,4.,
```

Sample of Output Data

```
        TIM       VBX       VBY       VBZ        XI        YI        ZI
     0.0000    0.0000  297.0000 -138.0000    0.0000    0.0000    0.0000

      THETA        VP
      .4345    4.0000

         BP        BL        VR
     4.1184    8.2368  327.4950

     4.1184    8.2368  327.4950


X-COORDS. OF NULL POINTS
         4.87        3.90        2.92        1.95         .97         .00        -.97       -1.95       -2.92       -3.90
        -4.87        4.87        3.90        2.92        1.95         .97         .00        -.97       -1.95       -2.92
        -3.90       -4.87        4.87        3.90        2.92        1.95         .97         .00        -.97       -1.95
        -2.92       -3.90       -4.87        4.87        3.90        2.92        1.95         .97         .00        -.97
        -1.95       -2.92       -3.90       -4.87        4.87        3.90        2.92        1.95         .97         .00
         -.97       -1.95       -2.92       -3.90       -4.87        4.87        3.90        2.92        1.95         .97
          .00        -.97       -1.95       -2.92       -3.90       -4.87        4.87        3.90        2.92        1.95
          .97         .00        -.97       -1.95       -2.92       -3.90       -4.87        4.87        3.90        2.92
         1.95         .97         .00        -.97       -1.95       -2.92       -3.90       -4.87        4.87        3.90
         2.92        1.95         .97         .00        -.97       -1.95       -2.92       -3.90       -4.87        4.87
         3.90        2.92        1.95         .97         .00        -.97       -1.95       -2.92       -3.90       -4.87
         4.87        3.90        2.92        1.95         .97         .00        -.97       -1.95       -2.92       -3.90
        -4.87


Y-COORDS. OF NULL POINTS
        -3.90       -3.90       -3.90       -3.90       -3.90       -3.90       -3.90       -3.90       -3.90       -3.90
        -3.90       -2.92       -2.92       -2.92       -2.92       -2.92       -2.92       -2.92       -2.92       -2.92
        -2.92       -2.92       -1.95       -1.95       -1.95       -1.95       -1.95       -1.95       -1.95       -1.95
        -1.95       -1.95       -1.95        -.97        -.97        -.97        -.97        -.97        -.97        -.97
         -.97        -.97        -.97        -.97        -.00        -.00        -.00        -.00        -.00        -.00
         -.00        -.00        -.00        -.00        -.00         .97         .97         .97         .97         .97
          .97         .97         .97         .97         .97         .97        1.95        1.95        1.95        1.95
         1.95        1.95        1.95        1.95        1.95        1.95        1.95        2.92        2.92        2.92
         2.92        2.92        2.92        2.92        2.92        2.92        2.92        2.92        3.90        3.90
         3.90        3.90        3.90        3.90        3.90        3.90        3.90        3.90        3.90        4.87
         4.87        4.87        4.87        4.87        4.87        4.87        4.87        4.87        4.87        4.87
         5.85        5.85        5.85        5.85        5.85        5.85        5.85        5.85        5.85        5.85
         5.85


Z-COORDS. OF NULL POINTS
         0.00        0.00        0.00        0.00        0.00        0.00        0.00        0.00        0.00        0.00
         0.00        0.00        0.00        0.00        0.00        0.00        0.00        0.00        0.00        0.00
         0.00        0.00        0.00        0.00        0.00        0.00        0.00        0.00        0.00        0.00
         0.00        0.00        0.00        0.00        0.00        0.00        0.00        0.00        0.00        0.00
         0.00        0.00        0.00        0.00        0.00        0.00        0.00        0.00        0.00        0.00
         0.00        0.00        0.00        0.00        0.00        0.00        0.00        0.00        0.00        0.00
         0.00        0.00        0.00        0.00        0.00        0.00        0.00        0.00        0.00        0.00
         0.00        0.00        0.00        0.00        0.00        0.00        0.00        0.00        0.00        0.00
         0.00        0.00        0.00        0.00        0.00        0.00        0.00        0.00        0.00        0.00
         0.00        0.00        0.00        0.00        0.00        0.00        0.00        0.00        0.00        0.00
         0.00        0.00        0.00        0.00        0.00        0.00        0.00        0.00        0.00        0.00
         0.00        0.00        0.00        0.00        0.00        0.00        0.00        0.00        0.00        0.00
         0.00
0 J=ELEMENT NUMBER
  X1,X2,X3,X4=X COORDINATES OF THE POINTS FORMING THE ELEMENTS
  Y1,Y2,Y3,Y4=Y COORDINATES OF THE POINTS FORMING THE ELEMENTS
  Z1,Z2,Z3,Z4=Z COORDINATES OF THE POINTS FORMING THE ELEMENTS
  UNX,UNY,UNZ-COMPONENTS OF THE UNIT NORMAL VECTOR
  XPNP,YPNP,ZPNP=COORDINATES OF THE NULL POINT IN REFERENCE COORDINATE SYSTEM


    J        X1        X2        X3        X4       UNX      XPNP
             Y1        Y2        Y3        Y4       UNY      YPNP
             Z1        Z2        Z3        Z4       UNZ      ZPNP

    1      4.87      4.39      4.39      4.87      0.00      4.43
          -4.39     -4.39     -3.41     -3.41      0.00     -3.90
           0.00      0.00      0.00      0.00      1.00      0.00
```

76.0000	2	4.39	3.41	3.41	4.39	0.00	3.90
77.0000		-4.39	-4.39	-3.41	-3.41	0.00	-3.90
78.0000		0.00	0.00	0.00	0.00	1.00	0.00
79.0000							
80.0000	3	3.41	2.44	2.44	3.41	0.00	2.92
81.0000		-4.39	-4.39	-3.41	-3.41	0.00	-3.90
82.0000		0.00	0.00	0.00	0.00	1.00	0.00
83.0000							
84.0000	4	2.44	1.46	1.46	2.44	0.00	1.95
85.0000		-4.39	-4.39	-3.41	-3.41	0.00	-3.90
86.0000		0.00	0.00	0.00	0.00	1.00	0.00
87.0000							
88.0000	5	1.46	.49	.49	1.46	0.00	.97
89.0000		-4.39	-4.39	-3.41	-3.41	0.00	-3.90
90.0000		0.00	0.00	0.00	0.00	1.00	0.00
91.0000							
92.0000	6	.49	-.49	-.49	.49	0.00	.00
93.0000		-4.39	-4.39	-3.41	-3.41	0.00	-3.90
94.0000		0.00	0.00	0.00	0.00	1.00	0.00
95.0000							
96.0000	7	-.49	-1.46	-1.46	-.49	0.00	-.97
97.0000		-4.39	-4.39	-3.41	-3.41	0.00	-3.90
98.0000		0.00	0.00	0.00	0.00	1.00	0.00
99.0000							
100.0000	8	-1.46	-2.44	-2.44	-1.46	0.00	-1.95
101.0000		-4.39	-4.39	-3.41	-3.41	0.00	-3.90
102.0000		0.00	0.00	0.00	0.00	1.00	0.00
103.0000							
104.0000	9	-2.44	-3.41	-3.41	-2.44	0.00	-2.92
105.0000		-4.39	-4.39	-3.41	-3.41	0.00	-3.90
106.0000		0.00	0.00	0.00	0.00	1.00	0.00
107.0000							
108.0000	10	-3.41	-4.39	-4.39	-3.41	0.00	-3.90
109.0000		-4.39	-4.39	-3.41	-3.41	0.00	-3.90
110.0000		0.00	0.00	0.00	0.00	1.00	0.00
111.0000							
112.0000	11	-4.39	-5.36	-5.36	-4.39	0.00	-4.87
113.0000		-4.39	-4.39	-3.41	-3.41	0.00	-3.90
114.0000		0.00	0.00	0.00	0.00	1.00	0.00
115.0000							
116.0000	12	4.87	4.39	4.39	4.87	0.00	4.63
117.0000		-3.41	-3.41	-2.44	-2.44	0.00	-2.92
118.0000		0.00	0.00	0.00	0.00	1.00	0.00
119.0000							
120.0000	13	4.39	3.41	3.41	4.39	0.00	3.90
121.0000		-3.41	-3.41	-2.44	-2.44	0.00	-2.92
122.0000		0.00	0.00	0.00	0.00	1.00	0.00
123.0000							
124.0000	14	3.41	2.44	2.44	3.41	0.00	2.92
125.0000		-3.41	-3.41	-2.44	-2.44	0.00	-2.92
126.0000		0.00	0.00	0.00	0.00	1.00	0.00
127.0000							
128.0000	15	2.44	1.46	1.46	2.44	0.00	1.95
129.0000		-3.41	-3.41	-2.44	-2.44	0.00	-2.92
130.0000		0.00	0.00	0.00	0.00	1.00	0.00
131.0000							
132.0000	16	1.46	.49	.49	1.46	0.00	.97
133.0000		-3.41	-3.41	-2.44	-2.44	0.00	-2.92
134.0000		0.00	0.00	0.00	0.00	1.00	0.00
135.0000							
136.0000	17	.49	-.49	-.49	.49	0.00	.00
137.0000		-3.41	-3.41	-2.44	-2.44	0.00	-2.92
138.0000		0.00	0.00	0.00	0.00	1.00	0.00
139.0000							
140.0000	18	-.49	-1.46	-1.46	-.49	0.00	-.97
141.0000		-3.41	-3.41	-2.44	-2.44	0.00	-2.92
142.0000		0.00	0.00	0.00	0.00	1.00	0.00
143.0000							
144.0000	19	-1.46	-2.44	-2.44	-1.46	0.00	-1.95
145.0000		-3.41	-3.41	-2.44	-2.44	0.00	-2.92
146.0000		0.00	0.00	0.00	0.00	1.00	0.00
147.0000							
148.0000	20	-2.44	-3.41	-3.41	-2.44	0.00	-2.92
149.0000		-3.41	-3.41	-2.44	-2.44	0.00	-2.92
150.0000		0.00	0.00	0.00	0.00	1.00	0.00
151.0000							
152.0000	21	-3.41	-4.39	-4.39	-3.41	0.00	-3.90
153.0000		-3.41	-3.41	-2.44	-2.44	0.00	-2.92
154.0000		0.00	0.00	0.00	0.00	1.00	0.00
155.0000							
156.0000	22	-4.39	-5.36	-5.36	-4.39	0.00	-4.87
157.0000		-3.41	-3.41	-2.44	-2.44	0.00	-2.92
158.0000		0.00	0.00	0.00	0.00	1.00	0.00
159.0000							
160.0000	23	4.87	4.39	4.39	4.87	0.00	4.63
161.0000		-2.44	-2.44	-1.46	-1.46	0.00	-1.95
162.0000		0.00	0.00	0.00	0.00	1.00	0.00
163.0000							
164.0000	24	4.39	3.41	3.41	4.39	0.00	3.90
165.0000		-2.44	-2.44	-1.46	-1.46	0.00	-1.95
166.0000		0.00	0.00	0.00	0.00	1.00	0.00
167.0000							
168.0000	25	3.41	2.44	2.44	3.41	0.00	2.92
169.0000		-2.44	-2.44	-1.46	-1.46	0.00	-1.95
170.0000		0.00	0.00	0.00	0.00	1.00	0.00
171.0000							
172.0000	26	2.44	1.46	1.46	2.44	0.00	1.95
173.0000		-2.44	-2.44	-1.46	-1.46	0.00	-1.95
174.0000		0.00	0.00	0.00	0.00	1.00	0.00
175.0000							
176.0000	27	1.46	.49	.49	1.46	0.00	.97
177.0000		-2.44	-2.44	-1.46	-1.46	0.00	-1.95
178.0000		0.00	0.00	0.00	0.00	1.00	0.00
179.0000							

180.0000	28	.49	-.49	-.49	.49	0.00	.00
181.0000		-2.44	-2.44	-1.46	-1.46	0.00	-1.95
182.0000		0.00	0.00	0.00	0.00	1.00	0.00
183.0000							
184.0000	29	-.49	-1.46	-1.46	-.49	0.00	-.97
185.0000		-2.44	-2.44	-1.46	-1.46	0.00	-1.95
186.0000		0.00	0.00	0.00	0.00	1.00	0.00
187.0000							
188.0000	30	-1.46	-2.44	-2.44	-1.46	0.00	-1.95
189.0000		-2.44	-2.44	-1.46	-1.46	0.00	-1.95
190.0000		0.00	0.00	0.00	0.00	1.00	0.00
191.0000							
192.0000	31	-2.44	-3.41	-3.41	-2.44	0.00	-2.92
193.0000		-2.44	-2.44	-1.46	-1.46	0.00	-1.95
194.0000		0.00	0.00	0.00	0.00	1.00	0.00
195.0000							
196.0000	32	-3.41	-4.39	-4.39	-3.41	0.00	-3.90
197.0000		-2.44	-2.44	-1.46	-1.46	0.00	-1.95
198.0000		0.00	0.00	0.00	0.00	1.00	0.00
199.0000							
200.0000	33	-4.39	-5.36	-5.36	-4.39	0.00	-4.87
201.0000		-2.44	-2.44	-1.46	-1.46	0.00	-1.95
202.0000		0.00	0.00	0.00	0.00	1.00	0.00
203.0000							
204.0000	34	4.87	4.39	4.39	4.87	0.00	4.63
205.0000		-1.46	-1.46	-.49	-.49	0.00	-.97
206.0000		0.00	0.00	0.00	0.00	1.00	0.00
207.0000							
208.0000	35	4.39	3.41	3.41	4.39	0.00	3.90
209.0000		-1.46	-1.46	-.49	-.49	0.00	-.97
210.0000		0.00	0.00	0.00	0.00	1.00	0.00
211.0000							
212.0000	36	3.41	2.44	2.44	3.41	0.00	2.92
213.0000		-1.46	-1.46	-.49	-.49	0.00	-.97
214.0000		0.00	0.00	0.00	0.00	1.00	0.00
215.0000							
216.0000	37	2.44	1.46	1.46	2.44	0.00	1.95
217.0000		-1.46	-1.46	-.49	-.49	0.00	-.97
218.0000		0.00	0.00	0.00	0.00	1.00	0.00
219.0000							
220.0000	38	1.46	.49	.49	1.46	0.00	.97
221.0000		-1.46	-1.46	-.49	-.49	0.00	-.97
222.0000		0.00	0.00	0.00	0.00	1.00	0.00
223.0000							
224.0000	39	.49	-.49	-.49	.49	0.00	.00
225.0000		-1.46	-1.46	-.49	-.49	0.00	-.97
226.0000		0.00	0.00	0.00	0.00	1.00	0.00
227.0000							
228.0000	40	-.49	-1.46	-1.46	-.49	0.00	-.97
229.0000		-1.46	-1.46	-.49	-.49	0.00	-.97
230.0000		0.00	0.00	0.00	0.00	1.00	0.00
231.0000							
232.0000	41	-1.46	-2.44	-2.44	-1.46	0.00	-1.95
233.0000		-1.46	-1.46	-.49	-.49	0.00	-.97
234.0000		0.00	0.00	0.00	0.00	1.00	0.00
235.0000							
236.0000	42	-2.44	-3.41	-3.41	-2.44	0.00	-2.92
237.0000		-1.46	-1.46	-.49	-.49	0.00	-.97
238.0000		0.00	0.00	0.00	0.00	1.00	0.00
239.0000							
240.0000	43	-3.41	-4.39	-4.39	-3.41	0.00	-3.90
241.0000		-1.46	-1.46	-.49	-.49	0.00	-.97
242.0000		0.00	0.00	0.00	0.00	1.00	0.00
243.0000							
244.0000	44	-4.39	5.36	-5.36	-4.39	0.00	-4.87
245.0000		-1.46	-1.46	-.49	-.49	0.00	-.97
246.0000		0.00	0.00	0.00	0.00	1.00	0.00
247.0000							
248.0000	45	4.87	4.39	4.39	4.87	0.00	4.63
249.0000		-.49	.49	.49	.49	0.00	-.00
250.0000		0.00	0.00	0.00	0.00	1.00	0.00
251.0000							
251.0000							
252.0000	46	4.39	3.41	3.41	4.39	0.00	3.90
253.0000		-.49	-.49	.49	.49	0.00	-.00
254.0000		0.00	0.00	0.00	0.00	1.00	0.00
255.0000							
256.0000	47	3.41	2.44	2.44	3.41	0.00	2.92
257.0000		-.49	-.49	.49	.49	0.00	-.00
258.0000		0.00	0.00	0.00	0.00	1.00	0.00
259.0000							
260.0000	48	2.44	1.46	1.46	2.44	0.00	1.95
261.0000		-.49	-.49	.49	.49	0.00	-.00
262.0000		0.00	0.00	0.00	0.00	1.00	0.00
263.0000							
264.0000	49	1.46	.49	.49	1.46	0.00	.97
265.0000		-.49	-.49	.49	.49	0.00	-.00
266.0000		0.00	0.00	0.00	0.00	1.00	0.00
267.0000							
268.0000	50	.49	-.49	-.49	.49	0.00	.00
269.0000		-.49	-.49	.49	.49	0.00	-.00
270.0000		0.00	0.00	0.00	0.00	1.00	0.00
271.0000							
272.0000	51	-.49	-1.46	-1.46	-.49	0.00	-.97
273.0000		-.49	-.49	.49	.49	0.00	-.00
274.0000		0.00	0.00	0.00	0.00	1.00	0.00
275.0000							
276.0000	52	-1.46	-2.44	-2.44	-1.46	0.00	-1.95
277.0000		-.49	-.49	.49	.49	0.00	-.00
278.0000		0.00	0.00	0.00	0.00	1.00	0.00
279.0000							
280.0000	53	-2.44	-3.41	-3.41	-2.44	0.00	-2.92
281.0000		-.49	-.49	.49	[illegible]	0.00	-.00
282.0000		0.00	0.00	0.00	0.00	1.00	0.00
283.0000							

284.0000	54	-3.41	-4.39	-4.39	-3.41	0.00	-3.90
285.0000		-.49	-.49	.49	.49	0.00	-.00
286.0000		0.00	0.00	0.00	0.00	1.00	0.00
287.0000							
288.0000	55	-4.39	-5.36	-5.36	-4.39	0.00	-4.87
289.0000		-.49	-.49	.49	.49	0.00	-.00
290.0000		0.00	0.00	0.00	0.00	1.00	0.00
291.0000							
292.0000	56	4.87	4.39	4.39	4.87	0.00	4.63
293.0000		.49	.49	1.46	1.46	0.00	.97
294.0000		0.00	0.00	0.00	0.00	1.00	0.00
295.0000							
296.0000	57	4.39	3.41	3.41	4.39	0.00	3.90
297.0000		.49	.49	1.46	1.46	0.00	.97
298.0000		0.00	0.00	0.00	0.00	1.00	0.00
299.0000							
300.0000	58	3.41	2.44	2.44	3.41	0.00	2.92
301.0000		.49	.49	1.46	1.46	0.00	.97
302.0000		0.00	0.00	0.00	0.00	1.00	0.00
303.0000							
304.0000	59	2.44	1.46	1.46	2.44	0.00	1.95
305.0000		.49	.49	1.46	1.46	0.00	.97
306.0000		0.00	0.00	0.00	0.00	1.00	0.00
307.0000							
308.0000	60	1.46	.49	.49	1.46	0.00	.97
309.0000		.49	.49	1.46	1.46	0.00	.97
310.0000		0.00	0.00	0.00	0.00	1.00	0.00
311.0000							
312.0000	61	.49	-.49	-.49	.49	0.00	.00
313.0000		.49	.49	1.46	1.46	0.00	.97
314.0000		0.00	0.00	0.00	0.00	1.00	0.00
315.0000							
316.0000	62	-.49	-1.46	-1.46	-.49	0.00	-.97
317.0000		.49	.49	1.46	1.46	0.00	.97
318.0000		0.00	0.00	0.00	0.00	1.00	0.00
319.0000							
320.0000	63	-1.46	-2.44	-2.44	-1.46	0.00	-1.95
321.0000		.49	.49	1.46	1.46	0.00	.97
322.0000		0.00	0.00	0.00	0.00	1.00	0.00
323.0000							
324.0000	64	-2.44	-3.41	-3.41	-2.44	0.00	-2.92
325.0000		.49	.49	1.46	1.46	0.00	.97
326.0000		0.00	0.00	0.00	0.00	1.00	0.00
327.0000							
328.0000	65	-3.41	-4.39	-4.39	-3.41	0.00	-3.90
329.0000		.49	.49	1.46	1.46	0.00	.97
330.0000		0.00	0.00	0.00	0.00	1.00	0.00
331.0000							
332.0000	66	-4.39	-5.36	-5.36	-4.39	0.00	-4.87
333.0000		.49	.49	1.46	1.46	0.00	.97
334.0000		0.00	0.00	0.00	0.00	1.00	0.00
335.0000							
336.0000	67	4.87	4.39	4.39	4.87	0.00	4.63
337.0000		1.46	1.46	2.44	2.44	0.00	1.95
338.0000		0.00	0.00	0.00	0.00	1.00	0.00
339.0000							
340.0000	68	4.39	3.41	3.41	4.39	0.00	3.90
341.0000		1.46	1.46	2.44	2.44	0.00	1.95
342.0000		0.00	0.00	0.00	0.00	1.00	0.00
343.0000							
344.0000	69	3.41	2.44	2.44	3.41	0.00	2.92
345.0000		1.46	1.46	2.44	2.44	0.00	1.95
346.0000		0.00	0.00	0.00	0.00	1.00	0.00
347.0000							
348.0000	70	2.44	1.46	1.46	2.44	0.00	1.95
349.0000		1.46	1.46	2.44	2.44	0.00	1.95
350.0000		0.00	0.00	0.00	0.00	1.00	0.00
351.0000							
352.0000	71	1.46	.49	.49	1.46	0.00	.97
353.0000		1.46	1.46	2.44	2.44	0.00	1.95
354.0000		0.00	0.00	0.00	0.00	1.00	0.00
355.0000							
356.0000	72	.49	-.49	-.49	.49	0.00	.00
357.0000		1.46	1.46	2.44	2.44	0.00	1.95
358.0000		0.00	0.00	0.00	0.00	1.00	0.00
359.0000							
360.0000	73	-.49	-1.46	-1.46	-.49	0.00	-.97
361.0000		1.46	1.46	2.44	2.44	0.00	1.95
362.0000		0.00	0.00	0.00	0.00	1.00	0.00
363.0000							
364.0000	74	-1.46	-2.44	-2.44	-1.46	0.00	-1.95
365.0000		1.46	1.46	2.44	2.44	0.00	1.95
366.0000		0.00	0.00	0.00	0.00	1.00	0.00
367.0000							
368.0000	75	-2.44	-3.41	-3.41	-2.44	0.00	-2.92
369.0000		1.46	1.46	2.44	2.44	0.00	1.95
370.0000		0.00	0.00	0.00	0.00	1.00	0.00
371.0000							
372.0000	76	-3.41	-4.39	-4.39	-3.41	0.00	-3.90
373.0000		1.46	1.46	2.44	2.44	0.00	1.95
374.0000		0.00	0.00	0.00	0.00	1.00	0.00
375.0000							
376.0000	77	-4.39	-5.36	-5.36	-4.39	0.00	-4.87
377.0000		1.46	1.46	2.44	2.44	0.00	1.95
378.0000		0.00	0.00	0.00	0.00	1.00	0.00
379.0000							
380.0000	78	4.87	4.39	4.39	4.87	0.00	4.63
381.0000		2.44	2.44	3.41	3.41	0.00	2.92
382.0000		0.00	0.00	0.00	0.00	1.00	0.00
383.0000							
384.0000	79	4.39	3.41	3.41	4.39	0.00	3.90
385.0000		2.44	2.44	3.41	3.41	0.00	2.92
386.0000		0.00	0.00	0.00	0.00	1.00	0.00
387.0000							

388.0000	80	3.41	2.44	2.44	3.41	0.00	2.93
389.0000		2.44	2.44	1.41	1.41	0.00	2.93
390.0000		0.00	0.00	0.00	0.00	1.00	0.00
391.0000							
392.0000	81	2.44	1.46	1.46	2.44	0.00	1.95
393.0000		2.44	2.44	1.41	1.41	0.00	2.93
394.0000		0.00	0.00	0.00	0.00	1.00	0.00
395.0000							
396.0000	82	1.46	.49	.49	1.46	0.00	.97
397.0000		2.44	2.44	3.41	3.41	0.00	2.93
398.0000		0.00	0.00	0.00	0.00	1.00	0.00
399.0000							
400.0000	83	.49	-.49	-.49	.49	0.00	.00
401.0000		2.44	2.44	3.41	3.41	0.00	2.93
402.0000		0.00	0.00	0.00	0.00	1.00	0.00
403.0000							
404.0000	84	-.49	-1.46	-1.46	-.49	0.00	-.97
405.0000		2.44	2.44	1.41	1.41	0.00	2.93
406.0000		0.00	0.00	0.00	0.00	1.00	0.00
407.0000							
408.0000	85	-1.46	-2.44	-2.44	-1.46	0.00	-1.95
409.0000		2.44	2.44	3.41	1.41	0.00	2.93
410.0000		0.00	0.00	0.00	0.00	1.00	0.00
411.0000							
412.0000	86	-2.44	-3.41	3.41	-2.44	0.00	-2.93
413.0000		2.44	2.44	3.41	1.41	0.00	2.93
414.0000		0.00	0.00	0.00	0.00	1.00	0.00
415.0000							
416.0000	87	-3.41	-4.39	-4.39	-3.41	0.00	-3.90
417.0000		2.44	2.44	3.41	1.41	0.00	2.93
418.0000		0.00	0.00	0.00	0.00	1.00	0.00
419.0000							
420.0000	88	-4.39	-5.36	-5.36	-4.39	0.00	-4.87
421.0000		2.44	2.44	3.41	3.41	0.00	2.93
422.0000		0.00	0.00	0.00	0.00	1.00	0.00
423.0000							
424.0000	89	4.87	4.39	4.39	4.87	0.00	4.63
425.0000		3.41	3.41	4.39	4.39	0.00	3.90
426.0000		0.00	0.00	0.00	0.00	1.00	0.00
427.0000							
428.0000	90	4.39	3.41	1.41	4.39	0.00	1.90
429.0000		3.41	3.41	4.39	4.39	0.00	3.90
430.0000		0.00	0.00	0.00	0.00	1.00	0.00
431.0000							
432.0000	91	3.41	2.44	2.44	3.41	0.00	2.93
433.0000		3.41	3.41	4.39	4.39	0.00	3.90
434.0000		0.00	0.00	0.00	0.00	1.00	0.00
435.0000							
436.0000	92	2.44	1.46	1.46	2.44	0.00	1.95
437.0000		3.41	3.41	4.39	4.39	0.00	3.90
438.0000		0.00	0.00	0.00	0.00	1.00	0.00
439.0000							
440.0000	93	1.46	.49	.49	1.46	0.00	.97
441.0000		3.41	3.41	4.39	4.39	0.00	3.90
442.0000		0.00	0.00	0.00	0.00	1.00	0.00
443.0000							
444.0000	94	.49	-.49	.49	.49	0.00	.00
445.0000		1.41	1.41	4.39	4.39	0.00	3.90
446.0000		0.00	0.00	0.00	0.00	1.00	0.00
447.0000							
448.0000	95	-.49	-1.46	-1.46	-.49	0.00	-.97
449.0000		1.41	1.41	4.39	4.39	0.00	3.90
450.0000		0.00	0.00	0.00	0.00	1.00	0.00
451.0000							
452.0000	96	-1.46	-2.44	-2.44	-1.46	0.00	-1.95
453.0000		3.41	3.41	4.39	4.39	0.00	3.90
454.0000		0.00	0.00	0.00	0.00	1.00	0.00
455.0000							
456.0000	97	-2.44	-3.41	-3.41	-2.44	0.00	-2.93
457.0000		3.41	3.41	4.39	4.39	0.00	3.90
458.0000		0.00	0.00	0.00	0.00	1.00	0.00
459.0000							
460.0000	98	-3.41	-4.39	-4.39	3.41	0.00	-3.90
461.0000		1.41	1.41	4.39	4.39	0.00	3.90
462.0000		0.00	0.00	0.00	0.00	1.00	0.00
463.0000							
464.0000	99	-4.39	-5.36	-5.36	-4.39	0.00	-4.87
465.0000		1.41	3.41	4.39	4.39	0.00	3.90
466.0000		0.00	0.00	0.00	0.00	1.00	0.00
467.0000							
468.0000	100	4.87	4.39	4.39	4.87	0.00	4.63
469.0000		4.39	4.39	5.36	5.36	0.00	4.87
470.0000		0.00	0.00	0.00	0.00	1.00	0.00
471.0000							
472.0000	101	4.39	3.41	3.41	4.39	0.00	3.90
473.0000		4.39	4.39	5.36	5.36	0.00	4.87
474.0000		0.00	0.00	0.00	0.00	1.00	0.00
475.0000							
476.0000	102	3.41	2.44	2.44	3.41	0.00	2.93
477.0000		4.39	4.39	5.36	5.36	0.00	4.87
478.0000		0.00	0.00	0.00	0.00	1.00	0.00
479.0000							
480.0000	103	2.44	1.46	1.46	2.44	0.00	1.95
481.0000		4.39	4.39	5.36	5.36	0.00	4.87
482.0000		0.00	0.00	0.00	0.00	1.00	0.00
483.0000							
484.0000	104	1.46	.49	.49	1.46	0.00	.97
485.0000		4.39	4.39	5.36	5.36	0.00	4.87
486.0000		0.00	0.00	0.00	0.00	1.00	0.00
487.0000							
488.0000	105	.49	-.49	-.49	.49	0.00	.00
489.0000		4.39	4.39	5.36	5.36	0.00	4.87
490.0000		0.00	0.00	0.00	0.00	1.00	0.00
491.0000							

```
106      -.49    -1.46    -1.46    -.49    0.00    -.97
         4.39     4.39     5.36    5.36    0.00    4.87
         0.00     0.00     0.00    0.00    1.00    0.00

107     -1.46    -2.44    -2.44   -1.46    0.00   -1.95
         4.39     4.39     5.36    5.36    0.00    4.87
         0.00     0.00     0.00    0.00    1.00    0.00

108     -2.44    -3.41    -3.41   -2.44    0.00   -2.92
         4.39     4.39     5.36    5.36    0.00    4.87
         0.00     0.00     0.00    0.00    1.00    0.00

109     -3.41    -4.39    -4.39   -3.41    0.00   -3.90
         4.39     4.39     5.36    5.36    0.00    4.87
         0.00     0.00     0.00    0.00    1.00    0.00

110     -4.39    -5.36    -5.36   -4.39    0.00   -4.87
         4.39     4.39     5.36    5.36    0.00    4.87
         0.00     0.00     0.00    0.00    1.00    0.00

111      4.87     4.39     4.39    4.87    0.00    4.63
         5.36     5.36     6.33    6.33    0.00    5.85
         0.00     0.00     0.00    0.00    1.00    0.00

112      4.39     3.41     3.41    4.39    0.00    3.90
         5.36     5.36     6.33    6.33    0.00    5.85
         0.00     0.00     0.00    0.00    1.00    0.00

113      3.41     2.44     2.44    3.41    0.00    2.92
         5.36     5.36     6.33    6.33    0.00    5.85
         0.00     0.00     0.00    0.00    1.00    0.00

114      2.44     1.46     1.46    2.44    0.00    1.95
         5.36     5.36     6.33    6.33    0.00    5.85
         0.00     0.00     0.00    0.00    1.00    0.00

115      1.46      .49      .49    1.46    0.00     .97
         5.36     5.36     6.33    6.33    0.00    5.85
         0.00     0.00     0.00    0.00    1.00    0.00

116       .49     -.49     -.49     .49    0.00     .00
         5.36     5.36     6.33    6.33    0.00    5.85
         0.00     0.00     0.00    0.00    1.00    0.00

117      -.49    -1.46    -1.46    -.49    0.00    -.97
         5.36     5.36     6.33    6.33    0.00    5.85
         0.00     0.00     0.00    0.00    1.00    0.00

118     -1.46    -2.44    -2.44   -1.46    0.00   -1.95
         5.36     5.36     6.33    6.33    0.00    5.85
         0.00     0.00     0.00    0.00    1.00    0.00

119     -2.44    -3.41    -3.41   -2.44    0.00   -2.92
         5.36     5.36     6.33    6.33    0.00    5.85
         0.00     0.00     0.00    0.00    1.00    0.00

120     -3.41    -4.39    -4.39   -3.41    0.00   -3.90
         5.36     5.36     6.33    6.33    0.00    5.85
         0.00     0.00     0.00    0.00    1.00    0.00

121     -4.39    -5.36    -5.36   -4.39    0.00   -4.87
         5.36     5.36     6.33    6.33    0.00    5.85
         0.00     0.00     0.00    0.00    1.00    0.00

 IMPACT POINT IS ON ELEMENT   50

VALUES OF 1ST AND LAST X-ELEMENTS 0
     0.00000     0.00000
     0.00000     0.00000
  I       XPNP         VFI          UN          UNX
          YPNP         SOURCE       VN          UNY
          ZPNP         CP           WN          UNZ

  6       .0000        .6667       .0000       0.0000
        -1.8980        .4445       .6667       0.0000
         0.0000        .5555      -.0000       1.0000

 17       .0000        .7075       .0000       0.0000
        -2.9235        .6202       .7075       0.0000
         0.0000        .3798      -.0000       1.0000

 28       .0000        .8269       .0000       0.0000
        -1.9490        .6838       .8269       0.0000
         0.0000        .3162      -.0000       1.0000

 39       .0000        .8410       .0000       0.0000
         -.9749        .7413       .8410       0.0000
         0.0000        .2587      -.0000       1.0000

 50       .0000        .9042       .0000       0.0000
         -.0000        .8176       .9042       0.0000
         0.0000        .1824      -.0000       1.0000

 61       .0000        .9467       .0000       0.0000
          .9749        .8963       .9467       0.0000
         0.0000        .1037      -.0000       1.0000

 72       .0000        .9780       .0000       0.0000
         1.9490        .9564       .9780       0.0000
         0.0000        .0436      -.0000       1.0000

 83       .0000       1.0079       .0000       0.0000
         2.9235       1.0160      1.0079       0.0000
         0.0000       -.0160      -.0000       1.0000

```

```
597.0000  94      .0000      1.0720      .0000      0.0000
598.0000         3.8980      1.1491     1.0720      0.0000
599.0000         0.0000      -.1491     -.0000      1.0000
600.0000
601.0000  105     .0000      1.1432      .0000      0.0000
602.0000         4.0775      1.3070     1.1432      0.0000
603.0000         0.0000      -.3070     -.0000      1.0000
604.0000
605.0000  116     .0000       .1034      .0000      0.0000
606.0000         5.0469       .0336      .1034      0.0000
607.0000         0.0000       .9664     0.0000      1.0000
608.0000
609.0000
610.0000
611.0000  PRESSURES AT THE NULL POINTS
412.0000     1946.01    1943.45    1930.91    1861.42     961.31    1085.61     961.31    1861.42    1930.91    1943.45
413.0000     1947.82    1944.36    1932.21    1917.51    1835.53     657.30     742.36     657.80    1835.53    1912.51
414.0000     1937.71    1945.79    1941.54    1931.47    1894.50   [illegible]   601.63     418.00     611.61  [illegible]
415.0000     1894.30    1931.42    1943.61    1939.04    1924.45    1837.90     589.91     536.37     505.62     536.37
416.0000      589.91    1837.90    1924.45    1941.23    1937.98    1921.44    1821.86     275.13     335.56     358.51
417.0000      335.56     275.13    1821.86    1921.44    1940.94    1930.94    1924.30    1837.71    -100.05     108.31
418.0000      202.72     108.31    -100.05    1837.71    1924.30    1941.64    1941.15    1931.11    1894.15    1799.05
419.0000      -44.00      85.21     -44.00    1799.35    1894.15    1931.11    1943.41    1944.04    1932.31    1916.50
420.0000     1832.75    -100.24     -31.17     100.24    1832.75    1916.50    1937.21    1945.53    1946.46    1941.79
421.0000     1927.31    1857.40    -416.40    -291.39    -416.40    1857.40    1927.31    1941.79    1942.50    1948.51
422.0000     1945.57    1937.27    1911.14    1834.12    -599.93    1834.12    1911.14    1937.27    1945.57    1949.33
423.0000     1950.21    1948.51    1944.56    1936.64    1918.96    1888.45    1918.96    1936.64    1944.56    1948.51
424.0000     1950.63
```

REFERENCES

1. Barber, J.P. and J.S. Wilbeck, "The Characterization of Bird Impacts on a Rigid Plate: Part I," AFFDL-TR-75-5, January 1975.

2. Peterson, R.L. and J.P. Barber, "Bird Impact Forces in Aircraft Windshield Design," AFFDL-TR-75-150, March 1976.

3. Barber, J.P., H.R. Taylor, and J.S. Wilbeck, "Bird Impact Forces and Pressures on Rigid and Compliant Targets," AFFDL-TR-77-60, May 1978.

4. Wilbeck, J.S.,"Impact Behavior of Low Strength Projectiles," AFML-TR-77-134, July 1978.

5. Bauer, D.P. and J.P. Barber, "Experimental Investigation of Impact Pressures Caused by Gelatin Simulated Birds and Ice," UDR-TR-78-114, November 1978.

6. Boehman, L.I. and A. Challita, "A Model for Predicting Bird and Ice Impact Loads on Structures," UDR-TR-79-54.

☆U.S.Government Printing Office: 1979 — 657-002/109